Primary Frequency Control with Flywheel Energy Storage Technologies

by

Dario Peralta Moarry

A thesis
presented to the University of Waterloo
in fulfillment of the
thesis requirement for the degree of
Master of Applied Science
in
Electrical and Computer Engineering

Waterloo, Ontario, Canada, 2017

I hereby declare that I am the sole author of this thesis. This is a true copy of the thesis, including any required final revisions, as accepted by my examiners.

I understand that my thesis may be made electronically available to the public.

Abstract

Over the last decade, concerns about greenhouse gas emissions have increased. Different strategies have been developed to minimize those effects, leading to the development of renewable energy sources worldwide. In recent years, the deployment of solar photovoltaic and wind energy-based renewable generation technologies have been growing at a fast pace. The penetration of these technologies into the power system network introduces new challenges for frequency and voltage stability because of the intermittency of these energy sources, and the increasing risk of significant voltage/frequency variations.

The significant penetration of renewable sources requires fast regulation of the frequency deviations; hence, the implementation of primary frequency controls is necessary. There exists different techniques and strategies for primary frequency control, where governor regulation and under frequency load shedding are two of the best known, but these have several limitations regarding fast response. Thus, new control techniques based on energy storage systems, which are able to provide fast frequency control, are being studied. In this context, a flywheel energy storage (FES) system is studied and modeled in this thesis for frequency control in power systems, using the well-known software Dynamic Simulation Assessment Tool (DSATools)®, to allow researchers and practitioners to readily model FES in power system studies, particularly the Independent Electric System Operator (IESO) of Ontario.

The proposed FES DSATools® model is tested and compared using a previously proposed test system with a large wind energy system (WES), which creates significant frequency and voltage fluctuations due to its characteristics. The FES stores and delivers energy to the power system, as required by the network, through a back-to-back power electronic converter system. A frequency/speed limiter controller is used, considering the network frequency deviation and the FES rotational speed in the active control of the flywheel-side converter for active power control of the flywheel. A static var compensator (SVC) for voltage control is also studied. The presented studies consider disturbances from sudden changes in the wind speed, which affect the WES output active power, creating considerable problems for the test system's stability.

The simulation results suggest that the proposed FES model implemented on the system studied, provides effective primary frequency control, and it also improves the network voltage. Thus, the FES is shown to maintain system stability, increasing the operational efficiency of conventional and renewable generators.

Acknowledgements

First of all, I would like to acknowledge and thank all the invaluable support of my supervisors, Prof. Claudio Cañizares and Prof. Kankar Bhattacharya. I offer my deepest gratitude for their guidance during my graduate studies at the University of Waterloo. It has been an honour to work under their supervision and being able to learn from two excellent professionals, who are an example for our generation.

I also sincerely acknowledge all the professors who guided my studies by sharing their invaluable knowledge through outstanding lectures, in particular Prof. Mehrdad Kazerani, Prof. Fakhri Karray, and Prof. Mehrdad Pirnia. I also thank Prof. Mehrdad Kazerani and Prof. John Simpson-Porco for serving as my thesis readers.

My deepest gratitude to all friends and colleagues who helped me throughout my studies: Andres Arias, Gabriel Bacca, Behnam Tamimi, Bharat Solanki, Chioma Anierobi, Daniel Remón, David Romero, Edson Giraldi, Enrique Vera, Fabian Calero, Fabricio Ordoñez, Indrajit Das, Ivan Calero, Juan Carlos Muñoz, Mariano Arreaga, Abolfazl (Amir) Mosaddegh, Marten Pape, Mauricio Restrepo, Mostafa Farrokhabadi, Nafeesa Mehboob, Nitin Padmanabhan, Shubhalakshmi Shetty, Sofía Guzmán, Talal Alharbi, and William Mendieta. I am thankful for all their help and the friendly environment provided during this journey.

I would like to specially acknowledge SENESCYT in Ecuador, for giving me this opportunity by funding my Master's studies.

Dedication

This work is dedicated to my parents, Dario and Patricia; my sisters, Pierina and Nicole; and all my family, who have always given me their unconditional support. To my beloved wife, Gianella, who has accompanied me throughout this journey, being by my side, encouraging me to be a better human being; I love you.

Finally, I would like to dedicate this thesis especially to my son, Alexander, who gave me the special motivation to continue working tirelessly.

Thanks for all their support, which I could not have done without.

Table of Contents

List of Tables

List of Figures

List of Acronyms

AGC automatic generation control

AVR automatic voltage regulator

DAM day ahead market

BES battery energy storage

BESS Battery energy storage system

C-PCS control and power conditioning system

DFIG doubly-fed induction generator

DPC direct power control

DoD depth of discharge

DSATools Dynamic Simulation Assessment Tool

DTC direct torque control

ESS energy storage system

EST energy storage technology

FACTS flexible AC transmission system

FERC Federal Energy Regulatory Commission

FES Flywheel energy storage

FOC flux oriented control

GHG green house gas

H inertia mass constant

HVDC high-voltage direct-current

IESO Independent Electric System Operator

IM Induction Machine

ISO-NE Independent System Operator New England

LFC load-frequency control

NCIS Northern Chile Interconnected System

PFC primary frequency control

PI proportional-integral

PID proportional-integral-derivative

PLL Phase-locked loop

PM Permanent Magnet

PSAT Power flow and Short circuit Assessment Tool

PV photovoltaic

RES renewable energy sources

ROCOF rate of change of frequency

RTM real time market

SOC state of charge

SPMM surface permanent magnet machine

SST solid state transformer

SVC static var compensator

TES thermal energy storage

TSAT Transient Security Assessment Tool

TSC thyristor switched capacitor

TSR thyristor switched reactor

UDM User-Defined Model

UFLS under frequency load shedding

VSC voltage source converter

WES wind energy system

Nomenclature

Parameters

$\alpha_{Flywheel\_side}$	VSC_1 power angle
$\alpha_{Network\_side}$	VSC_2 power angle
β	WES pitch angle
$\gamma_{Flywheel\_side}$	VSC_1 modulation ratio
$\gamma_{Network\_side}$	VSC_2 modulation ratio
ω	rotor angular speed
ω_{SG}	Synchronous generator speed
$\omega_{R_{FES}}$	FES rotor speed
$\omega_{R_{SG}}$	Synchronous generator rotor speed
τ_D	Derivative time constant
$\tau_{f_{IV}}$	Internal voltage filter time constant
τ_{f_P}	Active power filter time constant
$\tau_{f_{V_{ac}}}$	V_{ac} filter time constant
τ_I	Integrator time constant
$\tau_{l_{V_{ac}}}$	V_{ac} control time constant
τ_L	Frequency filter time constant

$\tau_{A_{AG}}$	Additional derivative time constant
$\tau_{A_{AVR}}$	Filter time constant
$\tau_{A_{Gov}}$	Pilot servomotor time constant
$\tau_{A_{SVC}}$	SVC time constant
$\tau_{A_{WES}}$	Pitch controller time constant
$\tau_{B_{AG}}$	Additional integral time constant
$\tau_{B_{AVR}}$	Regulator time constant
$\tau_{B_{Gov}}$	Gate servo time constant
$\tau_{B_{SVC}}$	SVC time constant
$\tau_{C_{Gov}}$	Gate servomotor time constant
$\tau_{C_{SVC}}$	SVC time constant
$\tau_{D_{SVC}}$	SVC time constant
$\tau_{E_{SVC}}$	Filter time constant
$\tau_{F_{SVC}}$	Thyristor susceptance time constant
$\tau_{I_{WES}}$	WES integral gain
E_{f_o}	Initial field voltage
G_{MAX}	Maximum gate position
G_{MIN}	Minimum gate position
K_{ap}	Aerodynamic power coefficient
K_b	Wind turbine radius coefficient
$K_{D_{V_{ac}}}$	V_{ac} droop
K_G	Speed limiter proportional gain
$K_{I_{DC}}$	DC-link integral gain

$K_{I_{PLL}}$	Phase-locked loop integral gain
K_{I_P}	Active power integral gain
$K_{I_{Vac}}$	V_{ac} integral gain
$K_{P_{DC}}$	DC-link proportional gain
$K_{P_{IV}}$	Internal voltage proportional gain
$K_{P_{PLL}}$	Phase-locked loop proportional gain
K_{P_P}	Active power proportional gain
$K_{P_{Vac}}$	V_{ac} proportional gain
K_P	Frequency deviation proportional gain
K_{turb}	Ratio of mechanical and aerodynamic powers
$K_{G_{AG}}$	Additional proportional gain
$K_{I_{Gov}}$	Integral gain
$K_{P_{Gov}}$	Proportional gain
$K_{P_{SVC}}$	SVC proportional gain
$K_{P_{WES}}$	WES proportional gain
N_C	Number of TSC steps
N_L	Number of TSR steps
PG_{MAX}	Maximum active power
P_{rating}	Rated MW of a single unit
P_{WES}	WES active power
$R_{P_{Gov}}$	Permanent droop
V_{MAX}	Maximum AVR voltage
V_{MIN}	Minimum AVR voltage

V_T	Terminal voltage
V_w	Wind speed
V_{Bus_2}	SVC Terminal voltage

Chapter 1

Introduction

1.1 Motivation

The penetration of renewable energy sources (RES) have been increasing over the past decade, in good part because of commitments from governments to reduce green house gas (GHG) emissions. The increasing penetration of RES, which are highly intermittent and variable generation sources, introduces new challenges for the stability of the system frequency and voltage. Therefore, there is a need to develop controls and appropriate strategies to alleviate the impact of sudden fluctuations in the balance of active and reactive power between generation and demand, which is one of the primary responsibilities of system operators [1].

As seen in Figure 1.1, solar photovoltaic (PV) and wind resources accounted for approximately 12% of Ontario's installed generation capacity in 2016 [2]. The considerable growth of wind and solar PV is reflected in their share of total energy generation in Ontario in 2010 and 2016 in Figure 1.2; note that wind and solar generation have increased from 1.9% in 2010 to 7% in 2016.

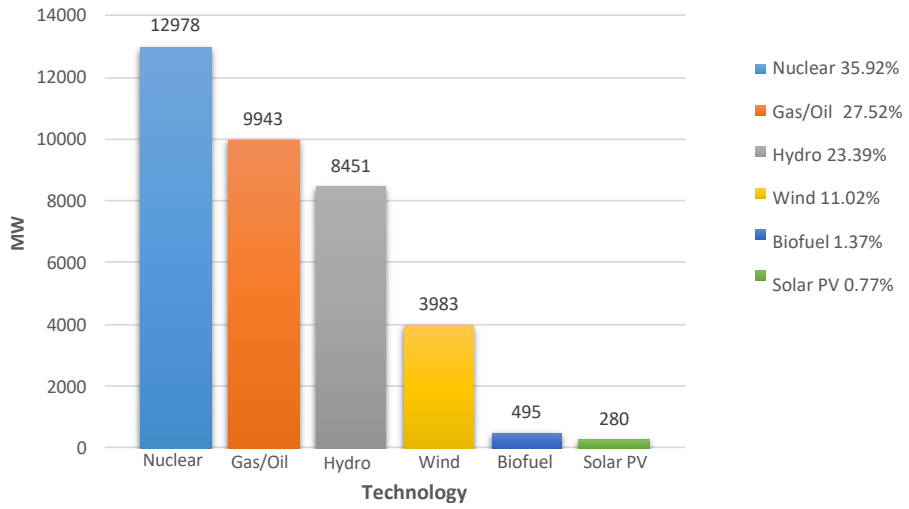

Figure 1.1: Installed generation capacity by technology in Ontario in 2016

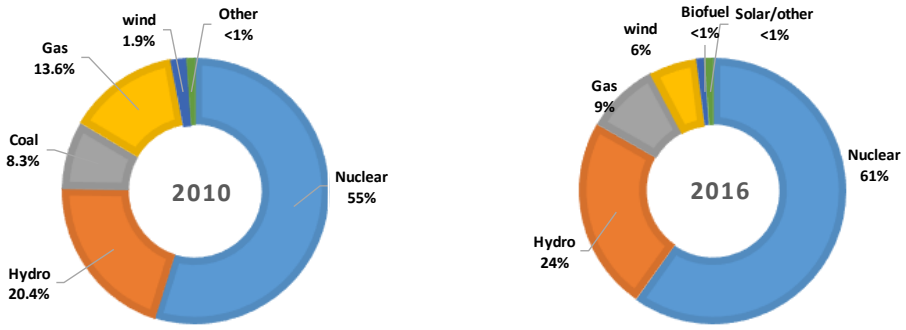

Figure 1.2: Energy output by generation technology in Ontario, in 2010 and 2016

Conventional control strategies, such as automatic generation control (AGC) and under frequency load shedding (UFLS), have limitations with respect to frequency regulation due to their slow response. Therefore, energy storage technologies (ESTs) have been found to be viable alternatives because of their intrinsic characteristics to attenuate the impact of intermittency and variability of RES with their fast-response attributes [3]. A 2 MW, 10-

flywheels based structure located in Minto, Ontario [4], and a 4 MW battery storage facility in London, Ontario [5], are the first operational EST installations in the province of Ontario that provide frequency regulation services. As of June 2017, the Independent Electric System Operator (IESO) of Ontario has entered contracted arrangements with private EST entities totaling 50 MW, to provide various ancillary services such as regulation, reactive power support, and reserves [6].

Flywheel energy storage (FES) technologies are particularly important, because of their fast response capability and high flexibility of operation [7,8]. However, not much work has been carried out on properly modeling the FES and analyze its performance. Therefore, the focus of this thesis is on developing a dynamic model, useful for the IESO, of an FES connected to a power system, to provide primary frequency control (PFC), and study its effects on system stability.

1.2 Literature Review

A brief review of the existing technical literature pertaining to the provision of frequency control ancillary services using different ESTs is presented next.

1.2.1 Frequency Control Services with Energy Storage Technologies

Researchers in [9] present the study of PFC provided by EST units in the French island of Guadeloupe, located in the Caribbean sea. The paper mentions that fast-response ESTs can mitigate the effect of intermittency, where RES such as wind and solar are significant. Thus, it is noted that for the purpose of providing PFC, short-term storage units with fast-time response devices can be used. In the proposed control strategy, the EST needs to be activated before UFLS, and it must be able to supply/absorb power until the frequency deviation is nullified, after which the EST unit is deactivated.

A novel strategy for EST to participate in frequency regulation is proposed in [10]. The control strategy is in two stages: in the first stage, the EST unit regulates its short-term power output based on the wind power prediction information; in the second stage, frequency feedback is used to adjust the EST power output to reduce the steady-state frequency deviations further. Since the power output can be regulated before frequency deviations happen, the speed of frequency regulation can be significantly improved. Simu-

lation of a wind power system is performed on a real-time digital simulator, and the results show the effectiveness of the proposed method.

Researchers in [11] present a new frequency response model with participation of wind farms and EST in the application of PFC. Based on this model, the maximum rate of change of frequency and maximum frequency deviation are calculated. The proposed frequency control method can provide an appropriate evaluation of the participation of wind energy system (WES) and EST in the short-term frequency control of isolated power systems, based on the following criteria: The frequency regulating capability of wind farms and conventional synchronous generators, such as reheat steam turbines, are utilized as much as possible; the EST unit is controlled to participate in short-term frequency regulation with the minimum possible capacity.

Researchers in [12] present a method to determine the optimal capacity of a battery energy storage (BES) to provide frequency control in isolated systems. Three different operating strategies to measure the performance of the BES unit, while providing frequency regulation, are studied. Thereafter, based on the selection of the best strategy, and with the objective to maximize the net present value, considering the capacity cost as the primary cost, the optimal BES sizing is obtained.

In [13], the cost associated with BES capacity and operation for frequency control applications is considered. A model predictive control algorithm is used for the optimal operation of BES and its performance in PFC is analyzed. In [14], the authors examine the effect on the lifetime of a lithium-ion based BES when used to provide frequency control. The state of charge (SOC) of the battery and the degradation behavior are taken into account, and different operating strategies are analyzed.

Researchers in [15] propose a multi-area load-frequency control (LFC) structure with the inclusion of BES, in coordination with either proportional-integral (PI) or proportional-integral-derivative (PID) controllers, highlighting the advantages compared with conventional controllers for LFC. The improvement obtained with BES in combination with conventional controllers is examined.

In [16], the performance of the 1 MW BES installation located in Dietikon, Switzerland, is presented. It is noted that the facility offers PFC and other ancillary services. The selection and advantages of lithium-ion based BES technology, due to their high efficiency and fast charging/discharging rates is discussed. The paper considers a high cycling efficiency to set the cycle in the middle of the rated power, with a limit of 50% for charging and discharging rates. Also, the benefits of using BES instead of must-run generators are discussed in the context of fast response and rotational inertia levels, considering that the BES unit does not affect the frequency response of the European power system. A variety

of recharging methods are mentioned and tested in the paper to reduce the effects of the SOC self-discharging rates due to the internal losses. The paper also presents the effects on the performance of the BES in the first two years of usage, considering cycling efficiency, ramp rate, and initial battery cell degradation.

In [17], the energy management strategy for the inclusion of a lithium-ion based BES in the Danish power system with wind penetration is presented. An appropiate frequency control scheme is developed taking into account its time response, lifetime, efficiency and cost savings. The basic operation of the BES is to provide PFC by delivering active power when the frequency is below the accepted lower bound, or absorb power when it is above the upper bound. When the frequency is within limits, the SOC of the battery is assumed to be around 70%; thus, the BES is able to operate equitably for PFC.

Studies concerning the feasibility of using a network of thermal energy storage (TES) units without centralized control as an effective secondary load are investigated in [18]. Individual units respond to changes in the system frequency by activating an appropriate number of heating elements to absorb the surplus energy during high wind events. The purpose is to model the dynamics of such a wind-diesel coordinated microgrid and the proposed self-regulating TES unit network considering the critical system parameters to define a region of optimal operation.

The review of the aforementioned works in the area of frequency control with EST discussed in this section reveals the need for further improvements to ensure a reliable and stable operation of the system. These papers show the wide range of applications developed in power systems with different ESTs to provide LFC and PFC for power systems and microgrids, which are the basis for the models and studies discussed in this thesis.

1.2.2 Frequency Control with Flywheel Energy Storage

The importance of introducing FES to perform frequency regulation because of its ability to deliver/absorb significant amounts of power within a very short time, is explained in [7]; it also highlights the advantages of using asynchronous machines in FES to offset the network frequency variations caused by wind power fluctuations in microgrids. The importance of a fast frequency response that FES could provide in coordination with other technologies for frequency regulation is highlighted in [8]. It proposes a control strategy for frequency regulation in a wind-diesel microgrid, with the participation of other energy sources. Researchers in [19] detail a field oriented control model on an induction machine based FES facility to provide frequency regulation, and evaluates its impact when the microgrid is either connected to the network or is on islanded operation.

Researchers in [20] emphasize the benefits of using FES for PFC, comparing its short-term response time with that of conventional generators providing ancillary service in deregulated markets. It also argues that the main benefit is the fast-time response capacity, which can reduce the imbalance between the load demand and the power supply, improving the performance of the system. The paper indicates that the proposed methodology, applied in an Independent System Operator New England (ISO-NE) field trial, is to designate the FES units to provide frequency regulation service before the conventional generators. The paper compares the performance of the proposed methodology with other conventional methods for regulation services. The results demonstrate that FES is 35% more effective in providing fast regulation than other providers.

Reference [21] proposes a novel control scheme for a FES converter; a 20 MW FES provides frequency regulation service to a smart grid with several RES units and conventional generators. The proposed scheme improves the system frequency response to disturbances. The validation of the proposed method is carried out on a 6-bus hybrid test system.

An optimal PFC service using FES in a day ahead market (DAM) and real time market (RTM) is developed in [22], using the PJM Interconnection system historical data. The paper highlights the technical characteristics of FES that are suitable for PFC, and how the use of this technology could be favorable for the stimulus offered by the Federal Energy Regulatory Commission (FERC). Futhermore, the paper considers the difficulty to provide proper service when its energy capacity is close to the upper/lower boundaries. Finally, it also considers the small size properties of the FES, finding that the offers need to be posted with zero prices either in the DAM for the maximum service provision, or in the RTM for additional service provision considering the latest information of the SOC of the FES.

Researches in [23] establish a fuzzy-logic based voltage/frequency control of an induction motor in a dc microgrid system using FES. Fuzzy reasoning controls are based on the nonlinear relationship between the average dc-link current of the inverter and the velocity change of the flywheel. Reference [24] presents an optimal sizing model of a coordinated FES-conventional generation system to provide LFC, in which a control strategy is proposed to maintain the SOC level within the normal operation boundaries with the adoption of a non-dominated sorting genetic algorithm based optimization technique.

Based on the above-mentioned literature review, there is a need for state-of-the-art FES based PFC models for power systems with considerable penetration of RES. Hence, in this thesis, a novel and practical FES system model to provide PFC support through voltage source converters (VSCs) is proposed, developed, and tested. In particular, the proposed FES model is shown to provide fast frequency control services, for effective PFC.

1.2.3 Modeling of FES for Power System Studies

In [25], the modeling of a FES and dc system is presented to compensate for wind power oscillations of a large scale WES connected through a high-voltage direct-current (HVDC) transmission system, using a two stage solid state transformer (SST) to enhance the power profile at the grid side. The proposed FES includes a low speed induction machine connected to the dc side of the HVDC system through a VSC. A decoupled vector control of the FES VSC, based on voltage oriented control, is implemented to manage the active and reactive power exchange between the FES and the low voltage side of the SST, generating the reference d-q current components for the VSC according to the FES active and reactive power references.

Researches in [26] propose the design of a low speed FES coupled to a variable-speed WES. The FES configuration comprises an induction machine for which a direct torque control (DTC) is proposed, and the effectiveness of the control is compared to a conventional flux oriented control (FOC). The mechanical part of the flywheel is modeled based on its maximum speed and the energy storage capacity parameters. The results in this paper show that DTC is a more effective control method than the FOC in terms of the active power delivered to the system.

In [27], a surface permanent magnet machine (SPMM)-based FES plant model is presented for electromechanical dynamic analysis. The dynamics of the flywheel, dc-link capacitor, and controllers are described. Four controllers are considered to regulate the FES active power output, flywheel SOC, dc-link voltage, and reactive power injection from the grid side converter. A 50 MW FES plant with a 50 flywheel array is tested in the Northern Chile Interconnected System (NCIS), and its impact on inter-area oscillation is evaluated for various scenarios of load and conventional/renewable generation. The impact of FES plant location on oscillation damping is also explored. The obtained results demonstrate that although the FES plant is controlled to provide PFC, if the FES is properly located, oscillation damping could be also improved.

In [28], a control strategy using a FES system to reduce the frequency variation in a small power system with high WES penetration is presented. The FES consists of a doubly-fed induction generator (DFIG), a flywheel mass, and a secondary excitation circuit for adjustable speed control. The secondary excitation circuit is connected to the power system through an ac-dc-ac VSC link. The FES VSC controls the active and reactive power exchange with the system, and the dc link voltage and the reactive power flowing into the secondary excitation system are controlled by the grid VSC. The frequency stabilization strategy is carried out with a reference signal controller which determines the active power reference to be injected to or absorbed from the system. The results demonstrate the

effectiveness of the FES strategy to provide frequency stabilization in a small power system; furthermore, it determines the ideal power capacity for the FES.

The review of the different works shows different approaches for the modeling of FES systems, for a variety of electrical machines and different configurations of converters, for several power system studies. Also, various features of FESs for direct power system control or coordination with a WES are demonstrated. However, none of these papers present an adequate practical model of FES for power system stability studies that can be readily implemented in popular commercial analysis tools, which is the focus of this thesis.

1.3 Research Objectives

Based on the literature review presented in the previous section, it is noted that there is a need to develop practical dynamic models and adequate controls to address system frequency control in power systems with significant penetration of RES using FES, particularly for studies using existing dynamic simulation commercial software. Thus, the following objectives are the fundamental drivers of the present work:

1. Develop and validate a dynamic model of a FES for the popular Dynamic Simulation Assessment Tool (DSATools)®, used by the IESO, to assess its impact on PFC performance.

2. Implement a state-of-art frequency and voltage control strategy in a converter-based FES model, considering the FES speed limiter, frequency deviation, and converter voltage controller.

3. Demonstrate and study frequency and voltage variations and control, and FES characteristics and performance in the realistic test system extracted from [28], with significant wind power penetration and variations.

1.4 Outline of the Thesis

Chapter 2 presents the background required for the development of the presented research. Thus, a general overview of frequency control definitions and mathematical models is presented first, followed by an overview of the prevailing energy storage systems (ESSs) for power system applications; in this context, brief discussions are presented of different ESTs,

highlighting the benefits of each, and outlining the suitability of FES to provide PFC. An extensive overview of the components and applications of FES models in power systems is then provided. Finally, a brief introduction to DSATools® core programs employed for the simulations is presented.

A detailed description of the proposed FES model and of all the components involved in its topology, along with a description of the components selected in DSATools® to model the FES system, are presented in Chapter 3. Also, the FES controls implemented and their inputs and outputs, and the criteria for selection of the system parameters, are reviewed.

In Chapter 4, the test system study cases, and the results obtained with DSATools®are presented and discussed. A detailed comparison of the results for the different cases, the challenges faced, and analysis of the system performance are also presented in this chapter.

Finally, in Chapter 5, the conclusions of the presented research, highlighting the advantages of the proposed FES model and its applications to power systems for PFC are presented. The main contributions of the research are also described, and future research directions and applications of the proposed model are discussed in this chapter.

Chapter 2

Background

This chapter outlines the basic concepts and analytical tools used for the presented research. First, a general synopsis of frequency control definitions and mathematical models are presented. Second, a general overview of ESTs for power system applications is presented, followed by a description of the foundations, models, and operation of BES and FES with a general discussion of their components and applications. Finally, the approach, techniques, and programs used for power system stability studies are briefly reviewed.

2.1 Primary Frequency Control (PFC)

Frequency stability is one of the three main areas in the study of system stability [29]; it deals with maintaining the balance between generation and demand, that could be affected due to sudden disturbances. Frequency control is classified as primary control, secondary control, and tertiary control [30, 31], which operate in the order of seconds, minutes, and hours, respectively.

- PFC is recognized as a fast frequency control, which operates in the first few seconds after an unexpected frequency change, via a fast-response generator, smart load, or energy storage unit. Figure 2.1 shows the three key points, marked A, B and C on the frequency plot, for PFC. Point A represents the system frequency immediately before the disturbance; point B is the maximum frequency drop before the frequency is addressed by the action of controls; and finally, point C is the steady-state frequency after the PFC stabilizes the frequency.

- Secondary control includes balancing functions with the inclusion of AGC. The time response in this case is in the order of minutes or faster, in certain cases. The AGC function is to restore the frequency to its nominal value (60 Hz).
- Tertiary control incorporates strategies to handle current and future frequency contingencies, such as deployment of additional generation resources.

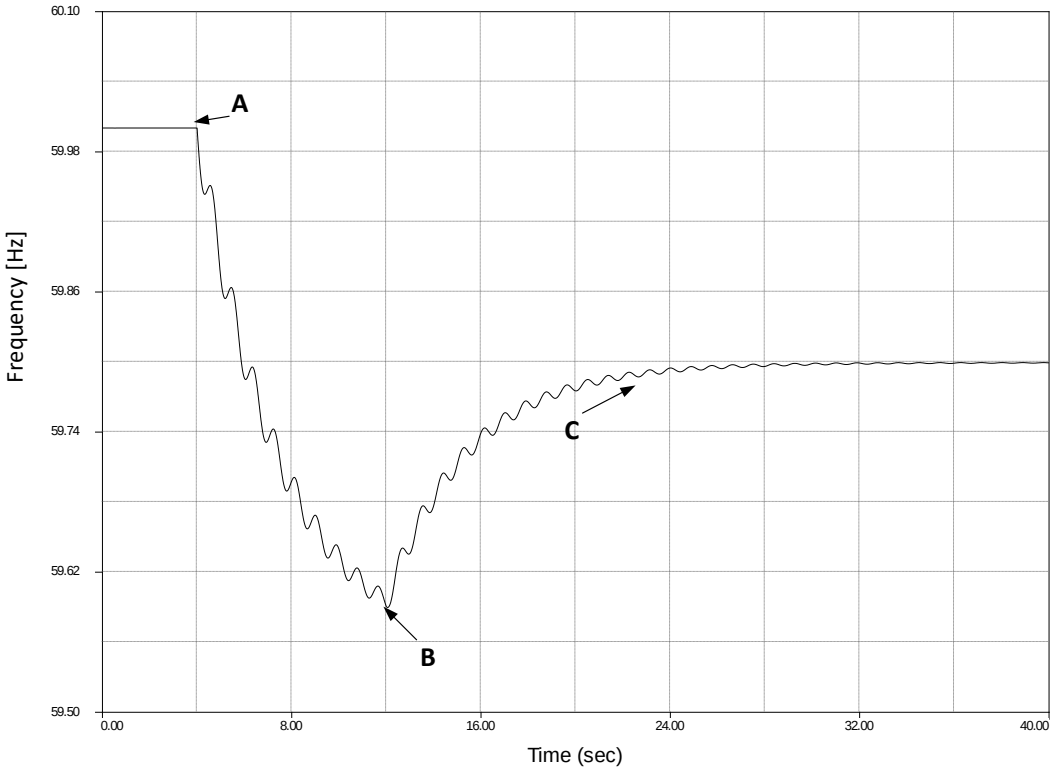

Figure 2.1: Frequency response with PFC.

The rate of change of frequency (ROCOF) can be calculated using the following relations:

$$\frac{d}{dt}\Delta f(t) = f_0 \frac{P_S(t) - P_D(t)}{2E} \tag{2.1}$$

$$H = \frac{E}{VA_{base}} \tag{2.2}$$

$$P_S^{PU}(t) - P_D^{PU}(t) = \Delta P_N^{PU}(t) \tag{2.3}$$

$$\frac{d}{dt}\Delta f(t) = f_0 \frac{\Delta P_N^{PU}(t}{2H} \tag{2.4}$$

where f_0 is the frequency before the disturbance; P_S and P_D are the power supply and demand, respectively; E is the kinetic energy stored in the rotating mass; and H is the inertia constant of the system [9].

In addition, the following constraints restricts the frequency variation within an acceptable range:

$$f_o - \Delta f_{max} \leq f \leq f_o + \Delta f_{max} \tag{2.5}$$

2.2 Energy Storage Technologies (ESTs)

Electrical energy cannot be stored but can be converted and stored in the form of chemical, kinetic, or thermal energy, using various ESTs [32–34]. ESSs store energy from the grid by conversion from electrical to any other form depending on the technology, using the energy directly when required, or injecting it back to the grid as electrical energy by re-conversion. The importance of including EST in power systems and the benefits that can be obtained regarding efficiency and safety are explained next.

The basic configuration of a small power system with ESS is given in Figure 2.2, in which it is observed that the ESS unit is connected to the system typically through a power electronic equipment such as a VSC. For large utility systems, the simultaneous use of two or more ESTs may be desirable; for example, TES and BES units could meet the power demand requirements over a 6 to 10 hour period, and provide short-time services over a 1 to 3 hour period, respectively [35].

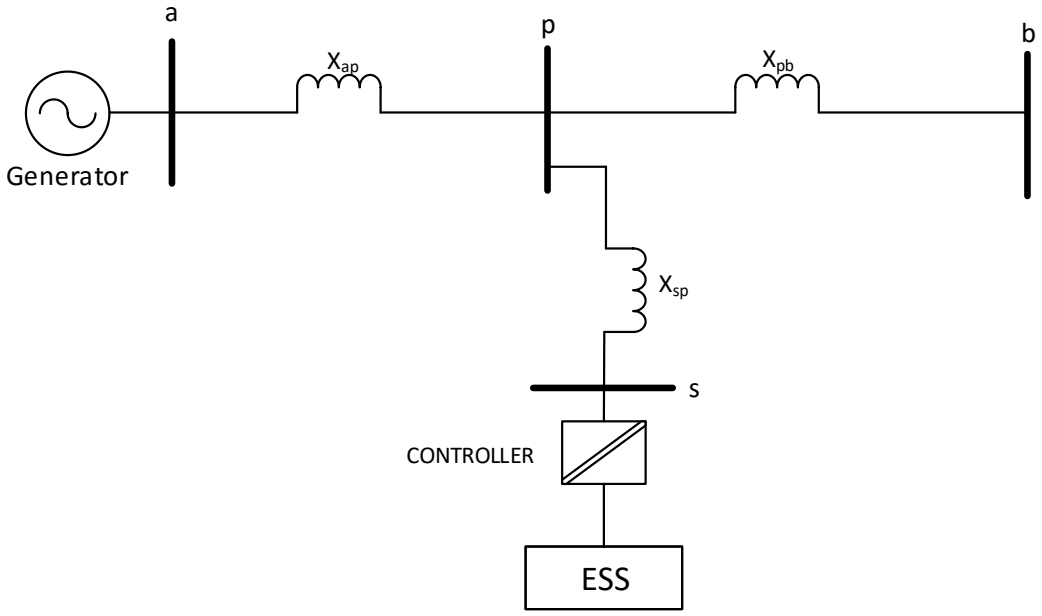

Figure 2.2: Small power system with ESS.

According to [36] some of the main advantages of ESTs for the power system include:

- Reduced energy costs,
- Increased flexibility of operation,
- Conservation of fossil fuel,
- Reduced pollutant emissions, and
- Lower maintenance costs.

The following sections present a review of the ESTs currently used by utilities for different power system applications, and the configuration, benefits, and basic models of each technology.

2.2.1 Battery Energy Storage System (BESS)

Battery energy storage systems (BESSs) store chemical energy and release it as electric energy on demand. It is a form of ESS and can be applied in high energy and high power applications. BESS are classified into three categories: conventional batteries, high-temperature, and flow batteries. Conventional batteries are based on the interaction of the cathode and anode electrodes in a reduction-oxidation reaction [35]. The materials most commonly used for the fabrication of batteries are the lead-acid, lithium-ion, nickel-cadmium, and sodium-sulfur.

- **Lead-Acid Battery:** The lead oxide at one electrode interacts with the sulfuric acid solution, which fills the cells; the released electrons flow through the circuit to the other electrode, generating electric current. When acting as a storage device, it can be recharged by a dc source, but it has a relatively short life. To avoid corrosion effects due to the solid electrodes, liquid electrodes could be designed; the most commonly used ones are made of sodium-sulfur, which not only reduces corrosion, but also increases the life of the battery [37].

- **Nickel-based Battery:** The most commonly used nickel-based batteries are made of nickel-zinc, nickel-iron, and nickel-cadmium alloys; the first two types have a short lifetime and a lower energy density. Nickel-cadmium batteries are quite different because they have high energy density and a longer lifetime. Also, they can be charged quickly, but one disadvantage is their tendency to overheat [38], which increases their cost, due to their need for refrigeration.

- **Lithium-Ion Battery:** The Li-ion battery has an alloy of aluminum and lithium as the negative electrode, and iron sulfide as the positive electrode (see Figure 2.3). For this type of battery, the electrolyte is made of molten salt, which is retained at temperatures above 350°C. It has a high energy and power density and a long life; however, it has a high cost and needs a ventilation system to reduce heating effects [39].

- **Sodium-Sulfur Battery:** In these batteries, the electrodes are liquid and the electrolyte is solid [35]. The main benefit is its long life, as compared to other types of batteries, which is due to the fact that liquids are much easier to reconstitute than solids.

High temperature batteries are commonly used with TES, due to their long energy storage duration and short time response. The most common high temperature-based

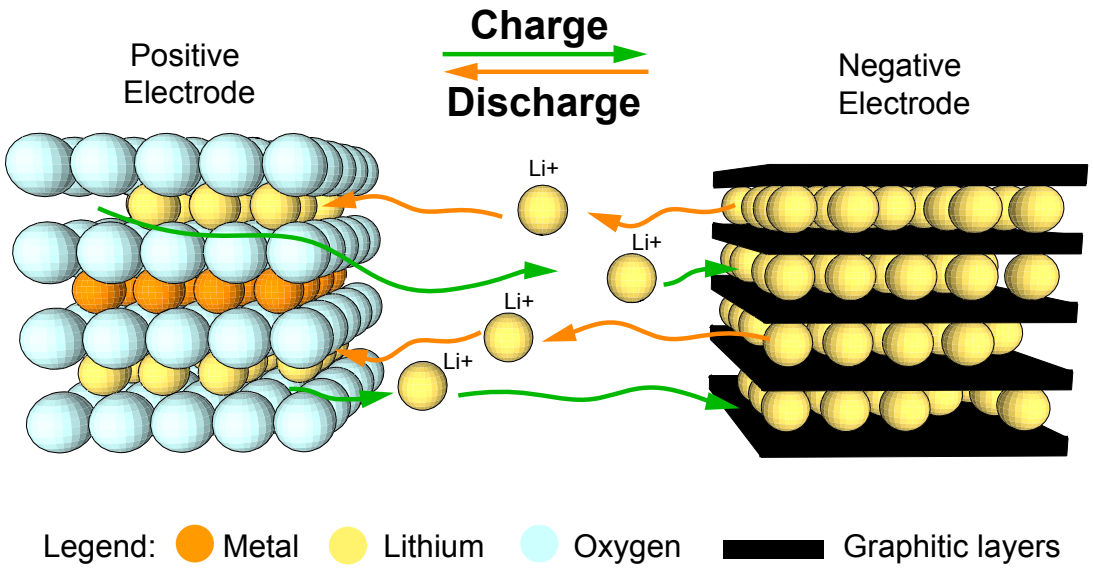

Figure 2.3: Lithium-ion battery components [35].

technologies are sodium sulfur and sodium nickel chloride batteries, with low-efficiency for the former.

Sodium and lithium batteries are the most preferred EST for ESS in power systems, but they have to be maintained at high temperatures to operate at maximum efficiency. Several types of batteries and their characteristics are listed in Table 2.1.

Flow batteries store the electrolyte material in external tanks that are pumped from the container to the cell stack; the use of this type of batteries is preferred for long duration charge/discharge processes. The general configuration is shown in Figure 2.4, depicting the ability of the battery to modify the energy and power capacity by varying the volume of the electrolyte, the number of cells, and the pump speed, respectively. The most common flow batteries are the hybrid flow and the vanadium redox flow batteries.

Table 2.1: Battery types and their properties.

Type	Specific ES capacity (W-h/Kg)	Lifetime cycles
Lead-acid (Pb)	29	1600
Nickel-cadmium (NiCd)	24	2000-3000
Nickel-iron (NiFe)	23	2000
Silver-zinc (AgZn)	185-220	200
Silver-zinc (AgCd)	110-165	500
Sodium-sulfur (NaS)	220	-
Lithium-chloride ($LiCl_2$)	440	-

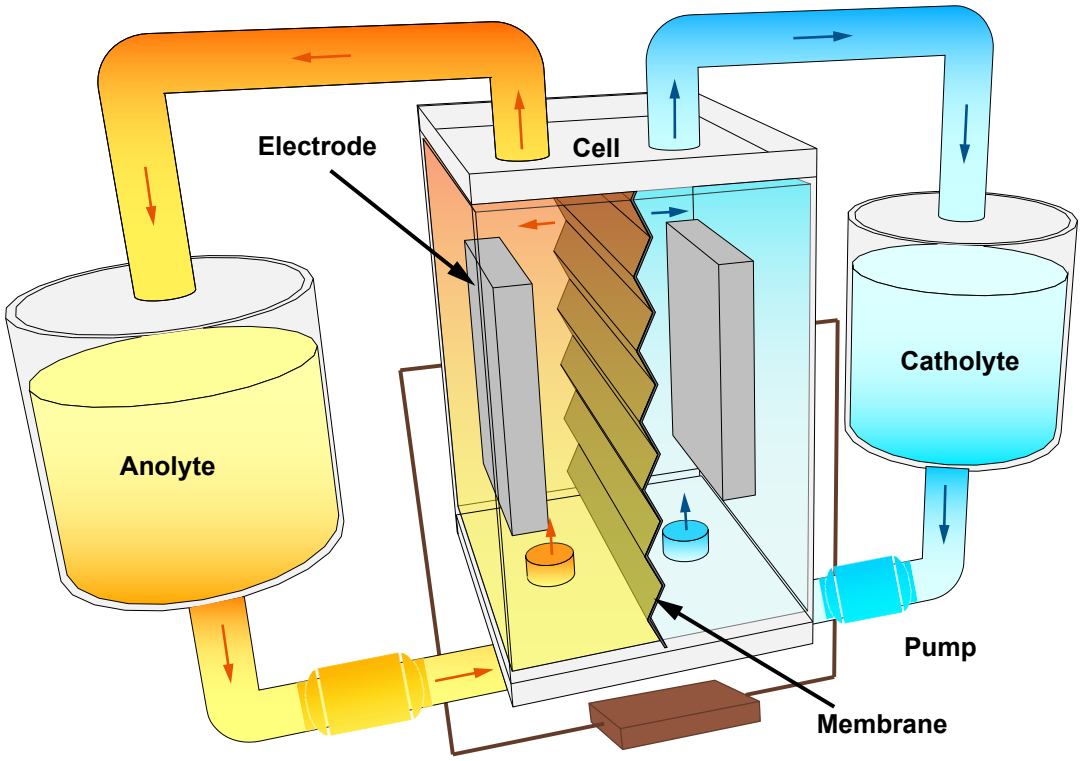

Figure 2.4: General configuration of a flow battery [35].

Each battery is characterized by its technical properties and benefits depending on the material. Lead-acid based BESSs are the most utilized design in power system applications; however, lithium-ion based BESSs have the highest efficiency [37].

A basic mathematical model of a BESS is given by:

$$E_{DCH} = \frac{\int P_{DCH} dt}{\eta_{DCH}} \tag{2.6}$$

$$E_{CH} = \eta_{CH} \int P_{CH} dt \tag{2.7}$$

$$SOC = SOC_0 \quad - \quad \frac{\int I_B dt}{C} \tag{2.8}$$

where E_{CH} and P_{CH} are the battery energy stored and power drawn during charging; E_{DCH} and P_{DCH} are the battery energy discharged and power injected during discharging; η_{CH} and η_{DCH} are the battery charging and discharging efficiencies, respectively; SOC_0 is the initial SOC of the battery; I_B is the battery current discharged to the grid ($I_B > 0$); and C is the battery capacity. For an extended battery life, it is desirable to maintain the battery SOC within a narrow range, effectively minimizing the depth of discharge (DoD).

One important component in the operation of BESS is the control and power conditioning system (C-PCS), which is the interface between the batteries and the electrical system, regulating the charge/discharge rates. The main components of the C-PCS, shown in Figure 2.5, are typically a dc-dc buck-boost converter that regulates the dc-link voltage, and a VSC that connects the BESS to the grid, which regulates the active and reactive power injected to or absorbed from the grid. The topology of the buck-boost converter is shown in Figure 2.6 [40].

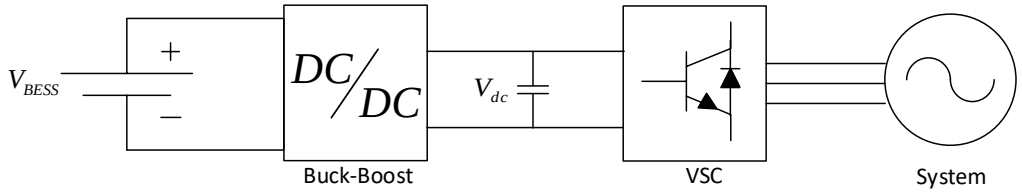

Figure 2.5: BES configuration.

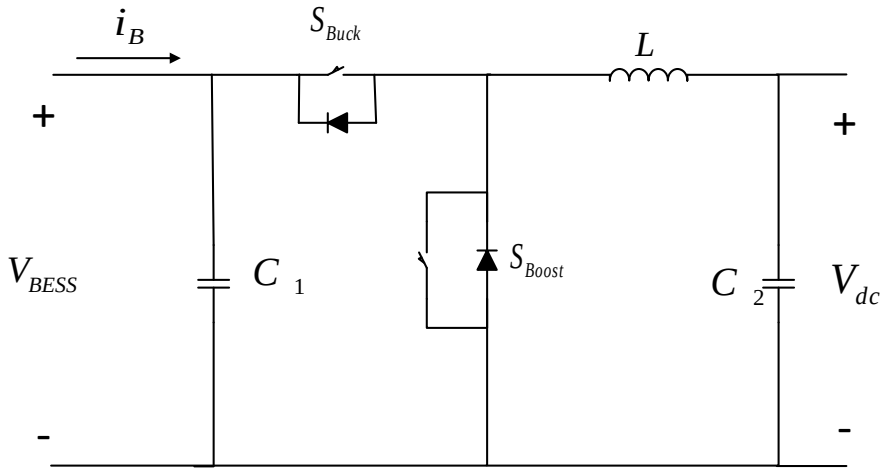

Figure 2.6: Buck-boost dc/dc converter topology [40].

2.2.2 Flywheel Energy Storage (FES)

FES converts electrical energy to rotational kinetic energy stored in a spinning mass. It comprises the rotor of the machine and the bearings enclosed in a vacuum to reduce the frictional torque caused by the very fast rotor speed [27, 35, 41]. The fast-response characteristic, and significant flexibility of FES allows for the provision of PFC in power systems, minimizing the considerable fluctuations of the active power injected by the variable gen-

eration [7].

The concept of FES is not new; its ability to provide a fast response to damping the impact of intermittency in power systems was recognized shortly after the invention of engines in the 19th century [36]; some decades later, it began to be considered for energy storage purposes. As it can be observed in Figure 2.7, some of the most important components of FES are the rotor and the stator. Other components such as the bearings and the material used in FES influence the efficiency of the device.

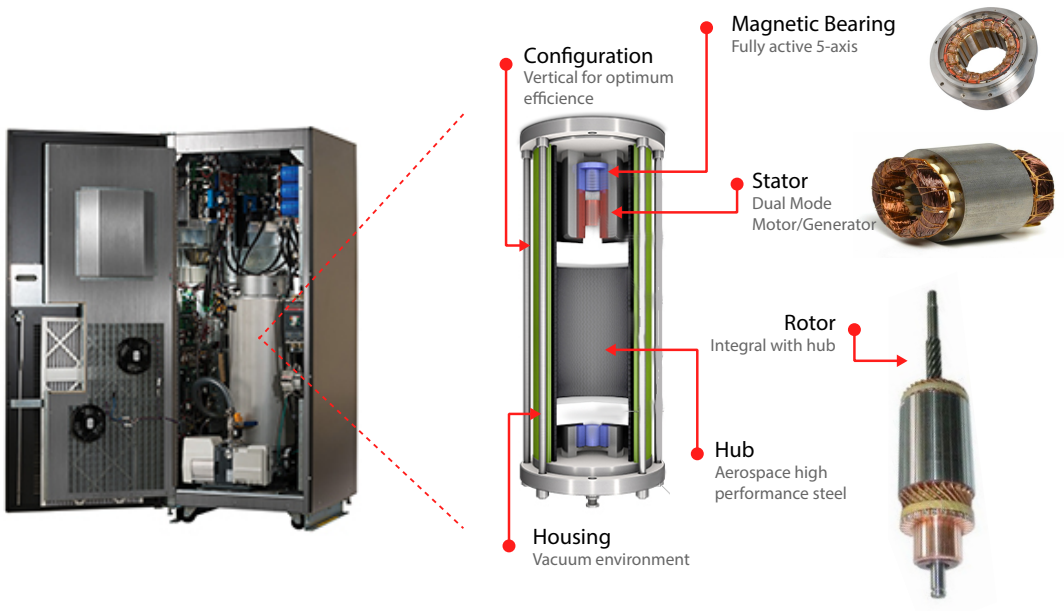

Figure 2.7: Basic FES device configuration [42].

The basic FES configuration, shown in Figure 2.8, consists of a flywheel driven by an electrical machine functioning as a motor/generator based on its mode of operation. The machine is interfaced to the power network through two bi-directional VSCs connected through a dc link. The topology of the VSCs corresponds to a full-bridge 3-phase converter, as shown in Figure 2.9. In Figure 2.8, VSC_1 controls the FES active power and the machine voltage, and VSC_2 controls the dc voltage and the terminal FES voltage.

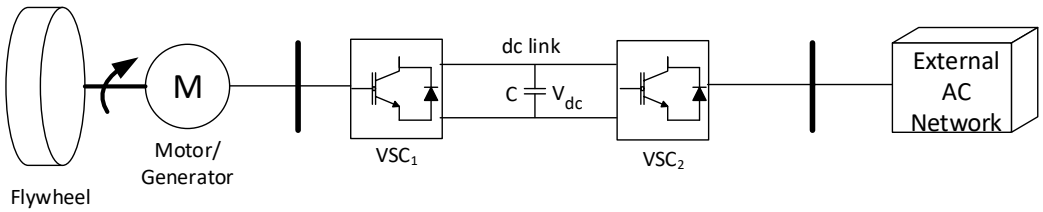

Figure 2.8: FES configuration [7].

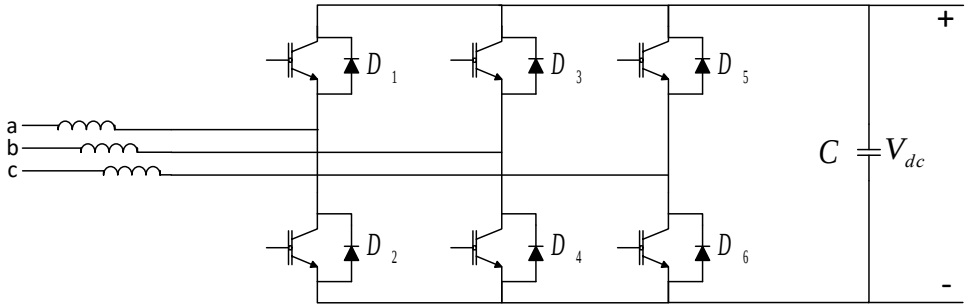

Figure 2.9: VSC topology [28].

Electric machines used with FES technologies are divided into three categories:

- **Induction Machines (IMs):** Both squirrel-cage and wound-rotor types of IMs can be utilized for low-speed high-power applications. Three control models can be implemented with IMs. Thus, DTC, FOC, and direct power control (DPC) operating with variable and constant switching frequency, respectively, can be used. Also, DPC could be implemented in power systems with considerable variation of active power.
- **Variable Reluctance Machines:** These machines are classified into two types, synchronous and switched reluctance machines, whose speed depends on the stator frequency and the number of poles, and the range of excitation switching between phases.
- **Permanent Magnet (PM) Machines:** There are two types of brush-less dc machines: PM synchronous machines, and the Halbach array machines; both types are

enclosed in vacuum. The optimal energy harvesting depends on their resistances as well as series resistors to control current-dependent losses.

The energy stored in the FES is given by [7]:

$$W = \frac{1}{2} J \omega_r^2 \tag{2.9}$$

$$J = m r^2 \tag{2.10}$$

where J is the combined moment of inertia of the rotor and load, and r and m are the radius and mass of the spinning mas, respectively. Given that the tensile strength of the material σ is related to the rotational speed ω_r as [7]:

$$\sigma = \rho r^2 {\omega_r}^2 \tag{2.11}$$

then:

$$W = \frac{1}{2} m \frac{\sigma}{\rho} \tag{2.12}$$

The basic machine electrical system is modeled as follows [7]:

$$\frac{d}{dt} i_d = \frac{1}{L_d} v_d - \frac{R}{L_d} i_d + \frac{L_q}{L_d} p \omega_r i_q \tag{2.13}$$

$$\frac{d}{dt} i_q = \frac{1}{L_q} v_q - \frac{R}{L_q} i_q + \frac{L_d}{L_q} p \omega_r i_d - \frac{\lambda p \omega_r}{L_q} \tag{2.14}$$

$$T_e = 1.5p \left[\lambda i_q + \left(L_d - L_q \right) i_d i_q \right] \tag{2.15}$$

where L_d and L_q are dq-axes inductances; R is the resistance of the stator winding; i_d and i_q are dq-axes currents; v_d and v_q are dq-axis voltages; ω_r is the angular velocity of the rotor; λ is the amplitude of the flux induced by the rotor in the stator phases; p is the number of pole pairs; and T_e is the electromagnetic torque. The mechanical system is modeled by the equations:

$$\frac{d}{dt}\omega_r = \frac{1}{J}(T_e - F\omega_r - T_m) \tag{2.16}$$

$$\frac{d\theta}{dt} = \omega_r \tag{2.17}$$

where F is the combined viscous friction of rotor and load, θ is the rotor angular position, and T_m is the mechanical torque.

The main FES characteristics are: fast charge/discharge rates, high power density, high energy density, low risk of overcharging/over-discharging, long life (up to 100,000 cycles or 20 years, approximately), and friendly environmental operation [43, 44]. FES installation and operation costs are lower than batteries and pumped storage technologies at the transmission level [45], and are used to control fast wind power variations, as in the case of Raglain mine [46], and for fast PFC in transmission systems, as in the case of Minto, Ontario [4].

2.3 DSATools®

DSATools® is a power system analysis software widely used at the IESO that offers a wide range of programs for power system planning and operational studies, with capabilities for comprehensive evaluation of system security, and includes all stability analysis techniques and tools. It consists of four core programs and a variety of add-on complementary tools. In the work presented in this thesis, two core programs and a complementary tool have been used for the presented dynamic studies and simulations; i.e., the Power flow and Short circuit Assessment Tool (PSAT)®, the Transient Security Assessment Tool (TSAT)®, and the User-Defined Model (UDM)® editor TSAT® add-on.

2.3.1 PSAT®

PSAT® is a program that can be used for stand-alone power flow analysis or data interchange with other DSATools® programs [47]. It is a graphical power flow program developed to perform steady state and contingency analysis. For these applications, the program allows for the organization of the system parameters, and also to choose from different methods to solve the power flow problem. The program also supports an extensive range of device models; for instance, three-winding transformers, flexible AC transmission

system (FACTS) components, switched shunt devices, HVDC links, VSCs, and negative and zero sequence networks for short circuit analysis. Model data can also be transferred from other software such as PSS/E and GE PSLF. The present work uses the Newton-Raphson method to solve the presented case studies.

2.3.2 TSAT®

TSAT® is a time-domain simulation tool designed for evaluation of the dynamic behavior of power systems [48]. TSAT® can be used to calculate transient security limits under specified criteria, contingencies, and transfer conditions. It is based on a nonlinear time-domain simulation engine that simulates accurately the dynamic behavior of power systems with various disturbances. It offers an extensive library of dynamic models of most power system devices.

The UDM® editor add-on, which is a module included in TSAT®, allows to represent a combination of device characteristics and control functions to facilitate the creation of control system models in a graphical environment [49]. In this thesis, the UDM® add-on is used to model the control systems of different equipment considered in the test system.

2.4 Summary

The background required to develop and test the proposed FES practical model was introduced in this chapter. A brief synopsis of frequency control techniques, mathematical models, and specific characteristics of PFC was presented, and an overview of ESTs and their applications for power systems was provided. Also, the main concepts, components, and applications of FES were described in some detail, as the basis for the dynamic modeling proposed in the next chapter. Finally, a brief discussion of DSATools®, which are used to develop and test the proposed FES practical model for dynamic and stability studies, was presented.

Chapter 3

Flywheel Energy Storage System Model

In this chapter, the components and controls of the FES practical model are discussed and developed for PFC applications in power systems. The FES model, comprises an induction machine, a flywheel represented as a high inertia mass constant (H), two bi-directional VSCs and all required controls, and is represented in the DSATools® [48, 49]. The proposed FES speed/frequency controls to provide PFC are presented in detail.

3.1 Components

3.1.1 Machine and Flywheel Model

The model selected for the dynamic representation of the induction machine configuration is the TSAT® MOT1G model, which represents a squirrel cage induction generator, with a high value of the parameter H to model the flywheel. This model was selected for its reliability and validity, and it represents either a generator or a motor, depending on the FES charging/discharging mode. The parameters selected for MOT1G for the simulation of the test system used here are presented in Table 3.1.

In charging mode, electrical energy is converted into mechanical energy and the rotational speed of the flywheel increases; in this case, in Figure 2.8, VSC_2 operates as a rectifier, while VSC_1 operates as an inverter, driving the machine as a motor. In discharging mode, mechanical energy of the rotating flywheel is converted into electrical energy via

the machine operating as a generator; in this case, the VSC_1 now operates as a rectifier, while VSC_2 operates as an inverter, at the network frequency, resulting in the rotational speed of the flywheel decreasing.

Table 3.1: Parameters of FES induction machine.

Parameter	**Value**
Transient rotor time constant [s]	0.4
Sub-transient rotor time constant [s]	0.1
Inertia [s]	19
Synchronous reactance [p.u.]	4.1
Stator resistance [p.u.]	0.01
Transient reactance [p.u.]	0.173
Sub-transient reactance [p.u.]	0.1
Stator leakage reactance [p.u.]	0.07
Field voltage (E1) [p.u.]	1.07
Saturation (E1) [p.u.]	0.5
Field voltage (E2) [p.u.]	1.06
Saturation (E2) [p.u.]	0.169

3.1.2 Voltage Source Converters

The VSCs are modeled in PSAT® and TSAT® as full-bridge, self-commutated 3-phase average converter models. For initial conditions, the network-side VSC_2 is assumed to be as a rectifier in PSAT®, and the flywheel-side VSC_1 is treated as an inverter; thus, the FES is considered to operate in charging mode for the Power flow analysis. The dc buses of the VSC units are connected through a dc link. The dc link is modeled as an LCL model, with two RL dc lines with a link capacitor. The controls are defined depending on the set points required in PSAT® studies to be performed; three specific control variables are defined for each VSC, which are: dc voltage, FES voltage, and modulation ratio for VSC_2; and FES active power, induction machine voltage, and modulation ratio for VSC_1. The parameters of the VSCs and the dc link are presented in Table 3.2 for the test system used here. A detailed description of the converter controls is given next.

Table 3.2: VSC converter data.

	Parameter	**Network VSC_2**	**Flywheel VSC_1**
Converter	Number of bridges	1	1
	Converter reactance [p.u.]	0.08	0.08
	DC to ac PWM gain [p.u.]	0.612	0.612
	Modulation ratio [p.u.]	0.5	0.5
	DC voltage link [kV]	4.0	
DC-link	link capacitance [μ F]	71.0	
	Line resistance [Ω]	0.02	0.02
	Line reactance [mH]	23.0	23.0

3.2 Controls

The FES controls developed and implemented are to control the rotor speed of the induction machine, and the frequency deviations. Also, the bi-directional VSC controls available in DSATools® are described next.

3.2.1 VSC Controls

The network-side VSC_2 maintains the dc link voltage constant at a reference value [25]. Figure 3.1 presents the control structure of the VSC_2, which controls the dc link voltage and the network ac voltage.

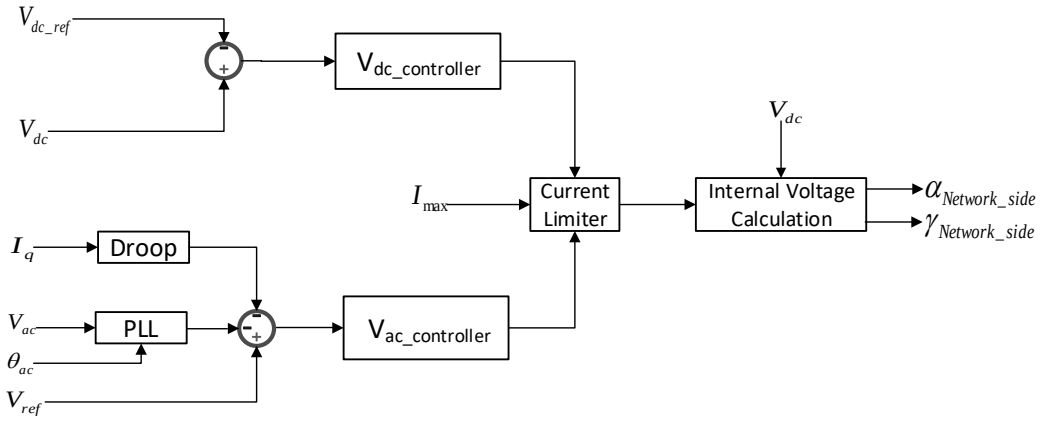

Figure 3.1: Network side converter (VSC_2).

The active power control shown in Figure 3.2, controls the flywheel-side by VSC_1. Note that the control topology is similar to the network-side VSC_2 controls, but instead of controlling the dc voltage, it controls the power injection to/from the flywheel; it also controls the ac voltage level of the FES induction machine.

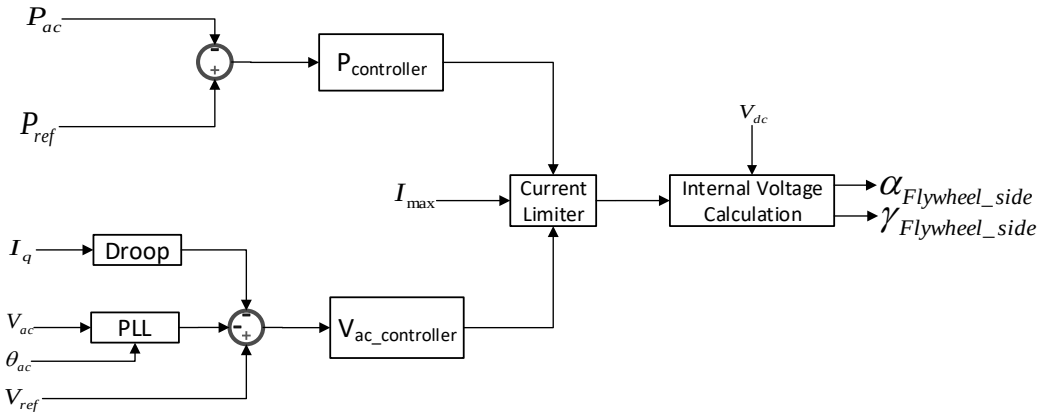

Figure 3.2: Flywheel side converter (VSC_1).

The power angle α and modulation ratio γ output signals of the VSC_1 and VSC_2 controls determine the active and reactive power exchanged with the corresponding ac

systems as follows [48]:

$$P = \frac{V_d V_c \gamma \sin(\alpha)}{X_c} \tag{3.1}$$

$$Q = \frac{V_d V_c \gamma \cos(\alpha)}{X_c} - \frac{V_c^2}{X_c} \tag{3.2}$$

where V_d is the converter dc voltages, V_c is the network voltage, and X_c is the converter reactance.

The VSC controls described here are available in the UDM® editor. Their parameters used for the simulations presented in this thesis are shown in Table 3.3

Table 3.3: VSC control parameters for Figures 3.1 and 3.2 [49].

Controller	**Parameter**	**Value**
V_{ac} controller (VSC$_1$ & VSC$_2$)	$\tau_{f_{V_{ac}}}$ [s]	0.00375
	$\tau_{l_{V_{ac}}}$ [s]	0.1
	$K_{P_{V_{ac}}}$ [p.u.]	0.6
	$K_{I_{V_{ac}}}$ [p.u.]	5.0
Droop (VSC$_1$ & VSC$_2$)	$K_{D_{V_{ac}}}$ [p.u.]	0.03
Internal voltage controller (VSC$_1$ & VSC$_2$)	$\tau_{f_{IV}}$ [s]	0.02
	$K_{P_{IV}}$ [p.u.]	1.11
Active power controller (VSC$_1$)	τ_{f_P} [s]	0.8
	K_{P_P} [p.u.]	0.3
	K_{I_P} [p.u.]	10
V_{dc} controller controller (VSC$_2$)	$K_{P_{DC}}$ [p.u.]	1.0
	$K_{I_{DC}}$ [p.u.]	100
Phase-locked loop (PLL) controller (VSC$_1$ & VSC$_2$)	$K_{P_{PLL}}$ [p.u.]	4.3
	$K_{I_{PLL}}$ [p.u.]	10

3.2.2 FES Speed/Frequency Control

The main purpose of the FES is to regulate and control the system frequency, which is accomplished here, with the proposed PFC given in Figure 3.3. The proposed control determines the active power reference P_{ref}, shown in Figure 3.2, in the active power control of the flywheel-side VSC to be injected to/from the FES, responding to the frequency deviations detected at the terminal of the system.

In an effort to prevent either the shortage or the surplus of energy stored in the FES, it is important to manage the rotor speed variation of the FES induction machine. Hence, a speed limiter is needed, as shown in Figure 3.3. The parameters selected for the speed/frequency control are given in Table 3.4.

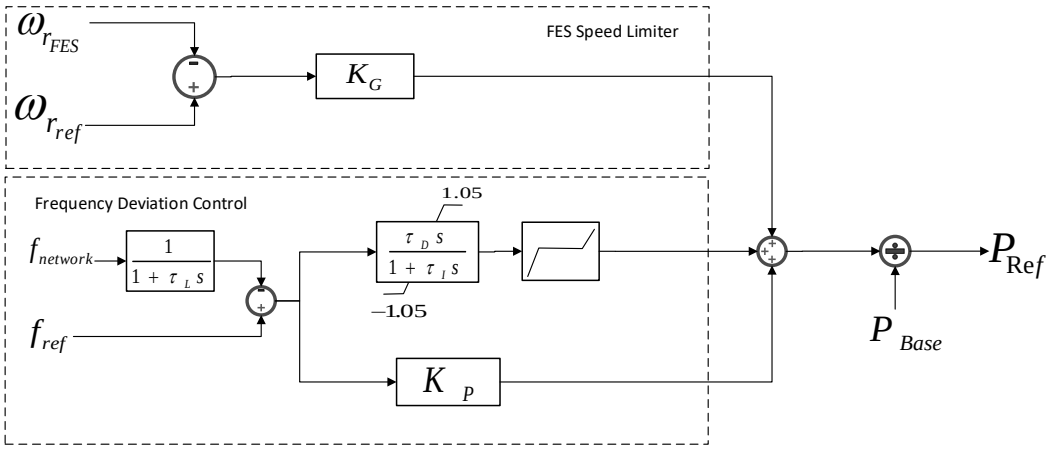

Figure 3.3: FES Speed/Frequency Control [28].

Table 3.4: FES Speed/Frequency Control parameters [28].

Parameter	**Value**
K_G [p.u.]	2.0
K_P [p.u.]	20.0
τ_L [s]	0.5
τ_D [s]	15.0
τ_I [s]	0.1

3.3 Summary

In this chapter, the DSATools® model of the components of the FES system were explained. The model selected for the FES induction machine and VSC, and their parameters were described. The topologies and parameters of the controls of the VSCs were also presented. Finally, a detailed explanation of the frequency/speed based control implemented to determine the active power to be injected into the FES unit to provide an appropriate PFC to the system was provided. In the next chapter, the proposed practical model and its application to PFC are presented through simulations and proper comparisons of various case studies on an existing FES test system.

Chapter 4

Simulation Test Systems and Results

This chapter presents an overview of the test system analyzed, with a brief description of the topology used. The performance of the FES system model for providing PFC, presented in Chapter 3, is evaluated and compared with the results obtained for the test system with no additional controllers, and with a static var compensator (SVC).

4.1 Test System Configurations

Three test system configurations considered are as follows:

- Case 1: Base system.
- Case 2: SVC system, i.e., Base system with the inclusion of an SVC.
- Case 3: FES system, i.e., Base system with the inclusion of the proposed FES model.

The test system used is extracted from [28], and is shown in Figure 4.1. This system is used here for model validation purposes and control impact studies. The Base system, modeled in DSATools®, is a balanced 3-phase system, with a synchronous generator acting as the principal source of energy of the grid, two resistive loads connected through a transmission line, and a WES based on a single induction generator, operating at almost constant speed. The configuration of the system in Case 2, shown in Figure 4.2, is the Base system with the addition of an SVC at Bus 2, where the WES is connected. Finally, the proposed FES system model discussed in Chapter 3 is added to the Base system at Bus 2, as illustrated in Figure 4.3.

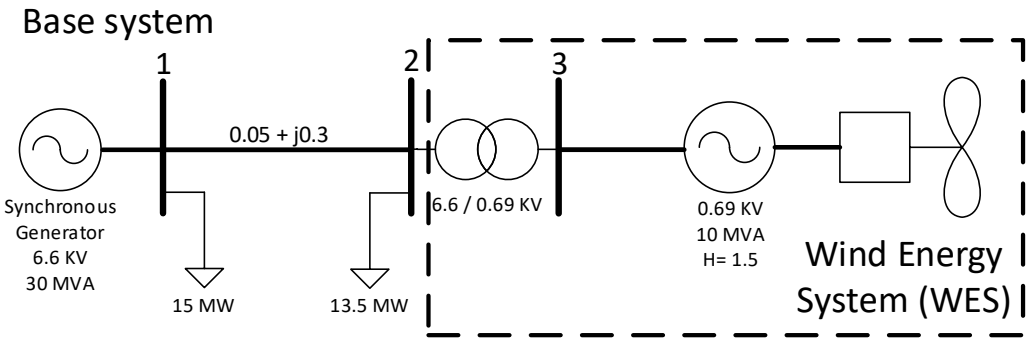

Figure 4.1: Base system configuration (Case 1).

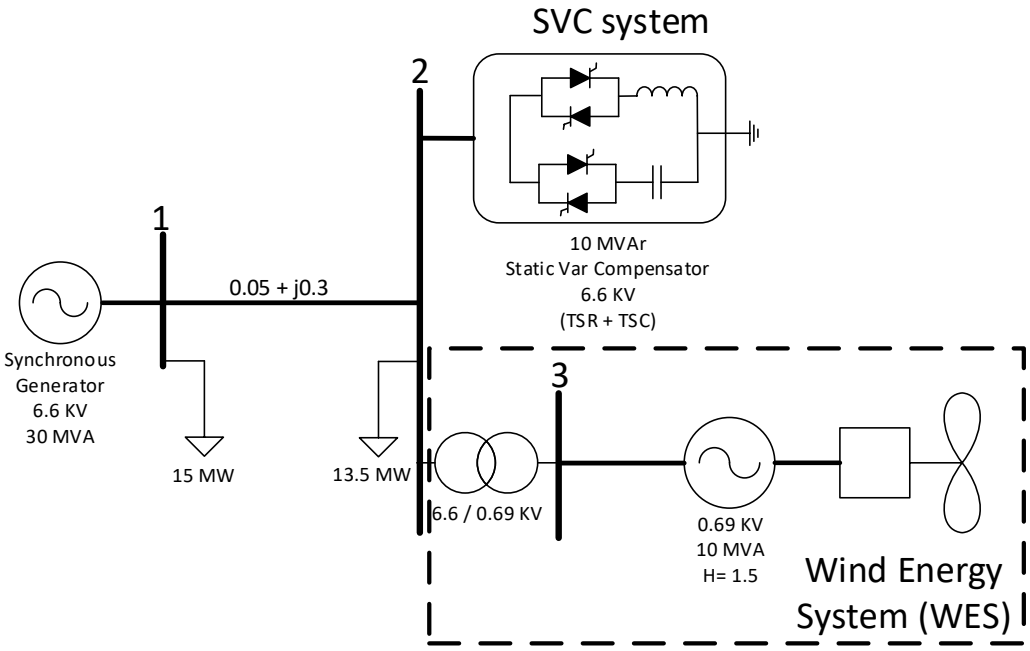

Figure 4.2: SVC system configuration (Case 2).

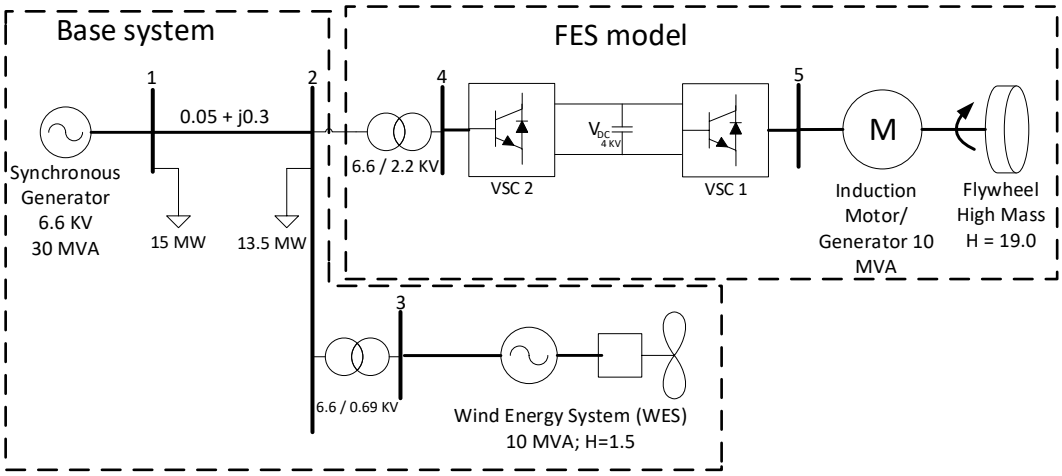

Figure 4.3: FES system configuration (Case 3).

4.1.1 Synchronous Generator Model

A synchronous generator is considered as the principal source of energy for the systems studied, and is modeled as a hydraulic power plant in TSAT®. A basic hydraulic turbine with Type 1 saturation model **DG1S1** is used [48], and the parameters are given in Table 4.1.

Table 4.1: Parameters of the synchronous generator.

Parameter	**Value**	
Capacity [MVA]	30	
Stator leakage reactance [p.u.]	0.14	
Armature resistance [p.u.]	0.0025	
Inertia [s]	2.5	
Field leakage reactance [p.u.]	0.2	
Field resistance [p.u.]	0.0004	
	D-axis	**Q-axis**
Magnetizing reactance [p.u.]	1.66	0.91
Damper winding leakage reactance [p.u.]	0.044	0.106
Damper winding resistance [p.u.]	0.005	0.0084

The plant gate is regulated by the governor control to maintain the turbine speed at a synchronous reference. The governor control was developed in the UDM® editor, using the **T22** type end-block diagram. Figure 4.4 shows the block diagram of the governor, and the parameter values are shown in Table 4.2

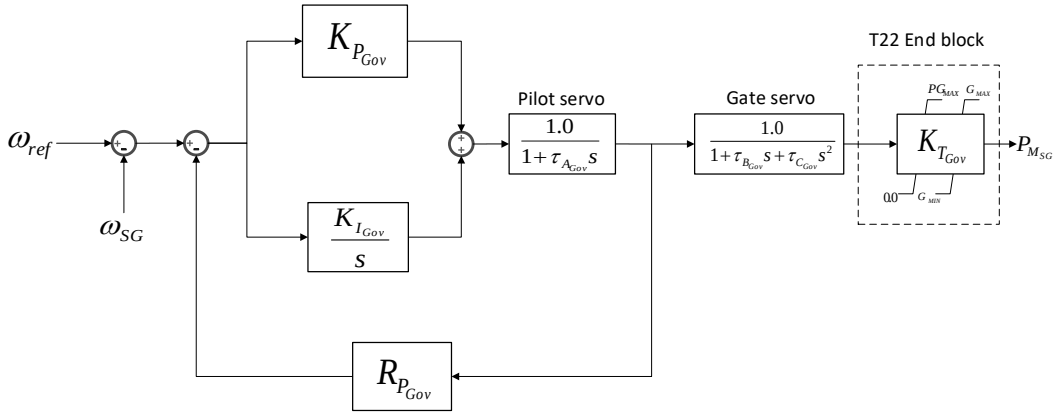

Figure 4.4: Synchronous generator governor block diagram [28].

Table 4.2: Synchronous generator governor control block [28].

Parameter	**Value**
$K_{P_{Gov}}$ [p.u.]	0.4
$K_{I_{Gov}}$ [p.u.]	0.1
$R_{P_{Gov}}$ [p.u.]	19
$\tau_{A_{Gov}}$ [s]	4.1
$\tau_{B_{Gov}}$ [s]	0.01
$\tau_{C_{Gov}}$ [s]	0.173
PG_{MAX} [p.u.]	1.0
G_{MAX}/G_{MIN} [p.u]	1.0/0.0
Additional governor control.	
$K_{G_{AG}}$ [p.u.]	0.1
$\tau_{A_{AG}}$ [s]	1.5
$\tau_{B_{AG}}$ [s]	0.1

Figure 4.5 shows the block diagram of the automatic voltage regulator (AVR) for the synchronous generator. The model is based on a simple AVR configuration in the UDM® editor, using the **E34** type end-block diagram. The parameters of the AVR are shown in Table 4.3

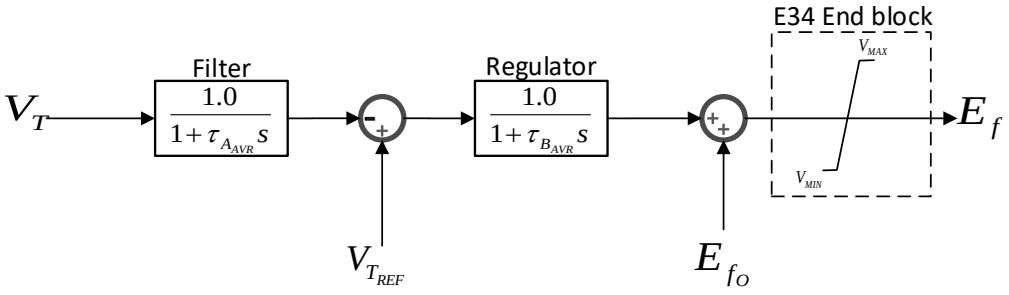

Figure 4.5: AVR block diagram [28].

Table 4.3: AVR control block [28].

Parameter	**Value**
$\tau_{A_{AVR}}$ [s]	0.01
$\tau_{B_{AVR}}$ [s]	0.01
V_{MAX}/V_{MIN} [p.u.]	5.0/-5.0

In Case 3, the FES controls the system frequency by injecting or absorbing active power through discharging and charging, respectively. In this case, the frequency would be controlled by the FES, and hence, the output signal of the synchronous generator torque does not change much, thus contributing little to frequency control. Therefore, a cooperative control, is added to the governor in [28] to avoid over charging/discharging of the FES. The block diagram of this control is presented in Figure 4.6, and the parameter values are shown in Table 4.2.

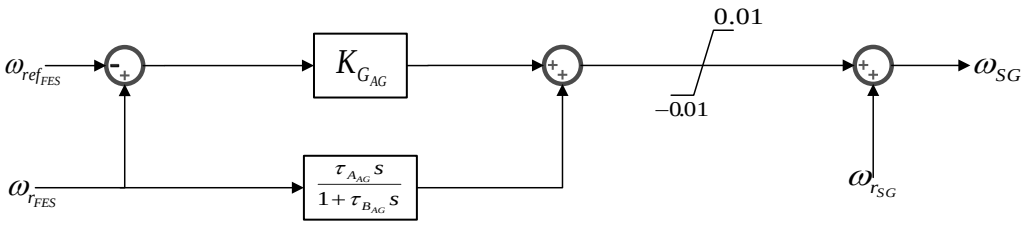

Figure 4.6: Additional governor control block diagram in Case 3 [28].

4.1.2 Wind Energy System (WES)

The WES consists of a squirrel cage induction generator and a wind turbine, represented in the **Wind Generator Model** end-block type. The parameters of the induction machine are given in Table 4.4.

Table 4.4: Parameters of WES induction machine [28].

Parameter	**Value**
Capacity [MVA]	10
Stator resistance [p.u.]	0.01
Stator leakage reactance [p.u.]	0.07
Magnetizing reactance [p.u.]	4.1
Rotor resistance [p.u.]	0.007
Rotor leakage reactance [p.u.]	0.07
H [s]	1.5

The mechanical power P_m, captured power C_p, and the aerodynamic characteristic λ_i and the tip speed ratio λ of the WES turbine blades are expressed by the following internal relations of the **WCP** block of the UDM® editor [49]:

$$P_m = \frac{K_{turb}\, K_{ap}\, V_w^3\, C_p(\lambda, \beta)}{P_{rating}} \tag{4.1}$$

$$C_p = 0.22\left[\frac{116}{\lambda_i} - 0.4\beta - 5\right] e^{\frac{-12.5}{\lambda_i}} \tag{4.2}$$

$$\frac{1}{\lambda_i} = \frac{1}{\lambda + 0.08\beta} - \frac{0.035}{\beta^3 + 1} \tag{4.3}$$

$$\lambda = \frac{K_b\, \omega_m}{V_w} \tag{4.4}$$

where K_{turb} is the ratio of aerodynamic power; K_{ap} is the equivalent coefficient of aerodynamic power; K_b is the equivalent wind turbine radius coefficient; V_w is the wind speed; P_{rating} is the rated power of the wind turbine; β is the pitch angle; and ω_m is the angular speed of the rotor. The values used here of these parameters are shown in Table 4.5.

Table 4.5: WES aerodynamic parameters [49].

Parameter	Value
K_{turb} [p.u.]	1.0
K_{ap} [p.u.]	0.00159
K_b [m]	56.6
P_{rating} [MW]	10

When the wind speed changes, the output power of the WES induction generator varies significantly, which causes a considerable disturbance on the grid. Hence, a conventional pitch angle controller β is used to maintain the output power of the induction generator within the rated power capacity, the output of the controller is included in the **WCP** control to obtain the P_m, and then, connected to the **wind generator model** to obtain the output active power of the WES. The block diagram of the controller is presented in Figure 4.7, and the parameters are provided in Table 4.6.

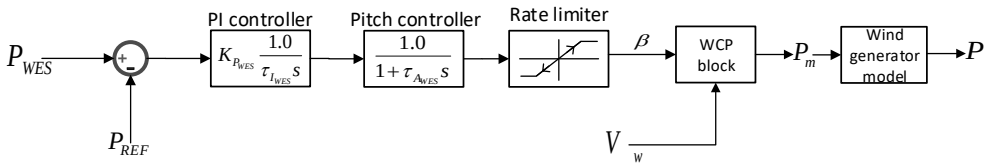

Figure 4.7: WES pitch angle controller [28].

Table 4.6: WES pitch angle controller parameters [28].

Parameter	Value
$K_{P_{WES}}$ [p.u.]	100
$\tau_{I_{WES}}$ [s]	0.01
$\tau_{A_{WES}}$ [s]	5.0

4.1.3 Static Var Compensator (SVC) model

The SVC model shown in Figure 4.8 is based on a thyristor switched capacitor (TSC), and a thyristor switched reactor (TSR). A first order susceptance B output control, with an

SD8 UDM® end-block diagram, is included to improve the quality of the voltage profile obtained in the Base system simulations. The parameters of this controller are shown in Table 4.7.

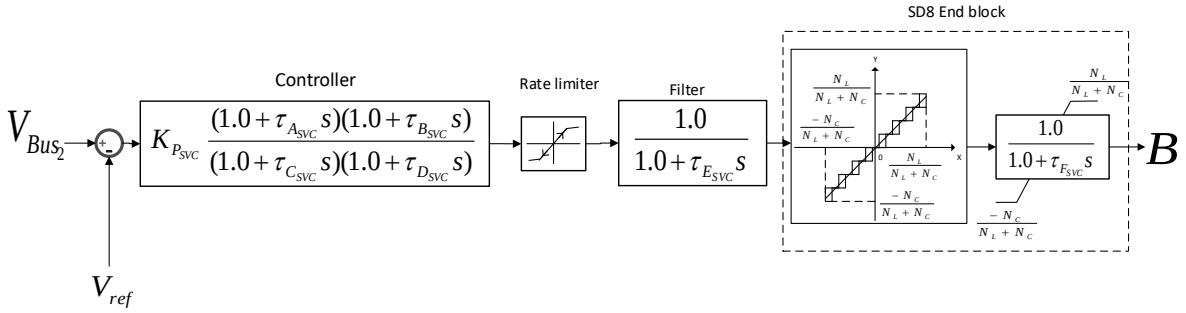

Figure 4.8: SVC controller [49].

Table 4.7: SVC controller [49].

Parameter	**Value**
$K_{P_{SVC}}$ [p.u.]	200
$\tau_{A_{SVC}}$ [s]	0.1
$\tau_{B_{SVC}}$ [s]	0.1
$\tau_{C_{SVC}}$ [s]	0.1
$\tau_{D_{SVC}}$ [s]	0.1
$\tau_{E_{SVC}}$ [s]	0.01
$\tau_{F_{SVC}}$ [s]	0.05
N_L	5
N_C	10

4.2 Simulation Results

Simulations of the three cases were carried out to validate the model and evaluate the contribution of the proposed FES system to frequency control, considering significant fluctuations of the wind speed in the first 100 s [28], with variations every 0.5 s, as shown in Figure 4.9. Thus assumed wind speed fluctuations affect the WES output active power, as shown in Figure 4.10, causing considerable variations in system frequency.

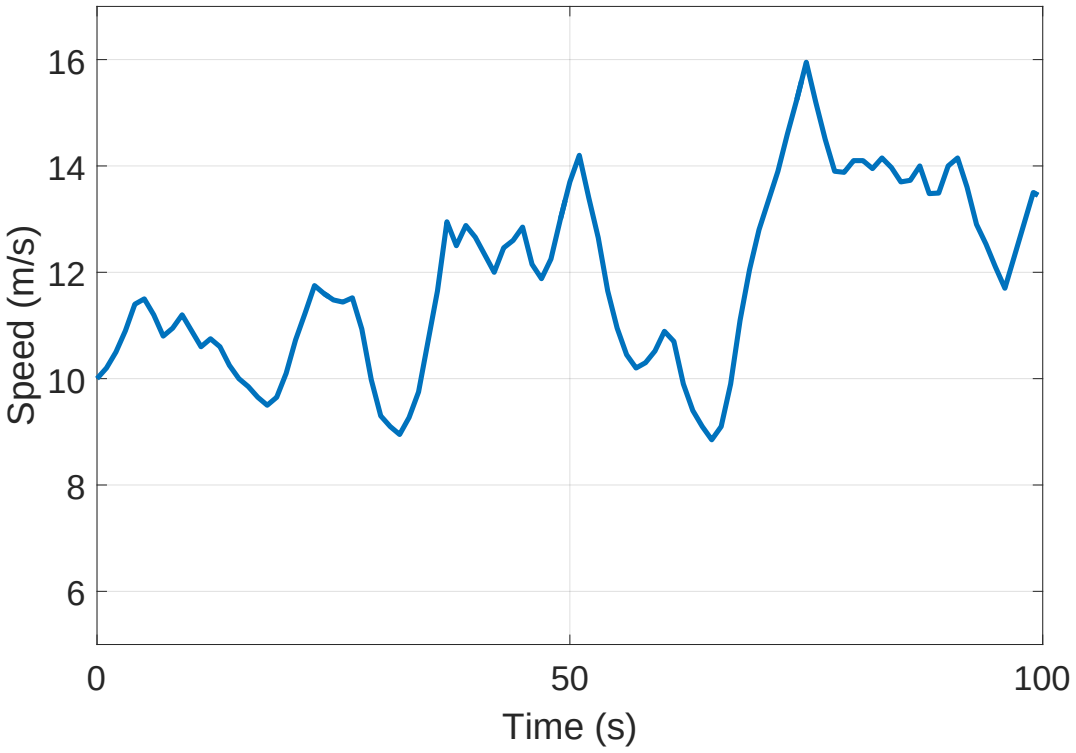

Figure 4.9: WES wind speed [28].

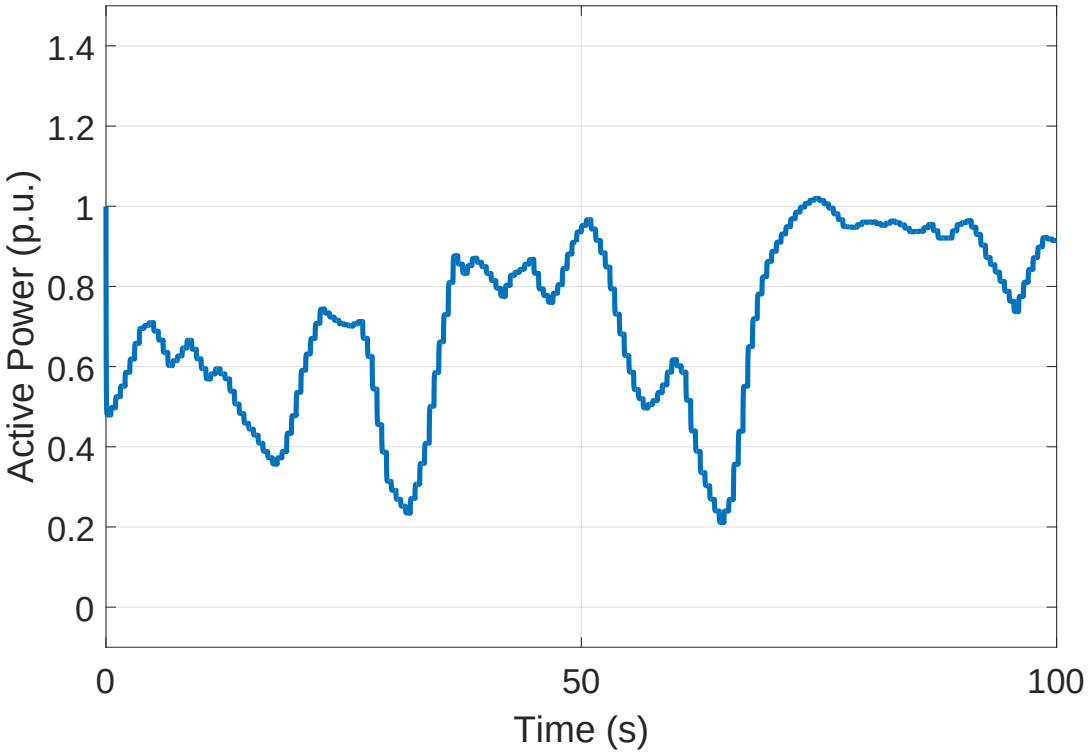

Figure 4.10: WES active power output.

4.2.1 System Frequency Response

Figure 4.11 presents the frequency response for the Base and FES systems considered; the nominal system frequency value is considered as 50 Hz for comparison with the results from [28]. Note that there is a significant improvement in the frequency response for the FES system as compared to the Base system, in which the frequency varies significantly, thus making the Base system unstable. Observe that for the Base system, there is a maximum frequency deviation of 3.1 Hz at t = 70s, whereas for the FES system this is reduced to 0.15 Hz, hence ensuring frequency stability of the system.

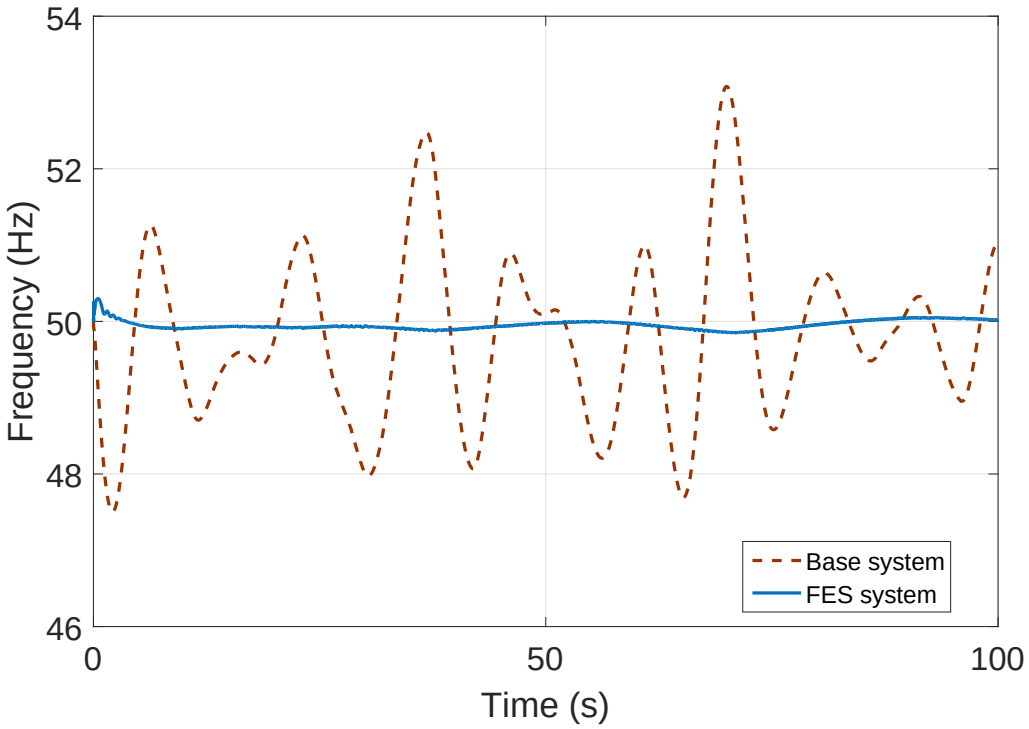

Figure 4.11: Test system frequency response.

4.2.2 Voltage Profiles

Figure 4.12 presents the voltage profile at Bus 1, observe that for both SVC and FES systems, the voltage fluctuations are reduced in comparison to the Base system, and the voltage level is increased to its nominal value; the FES system yields the best voltage profile among the three cases.

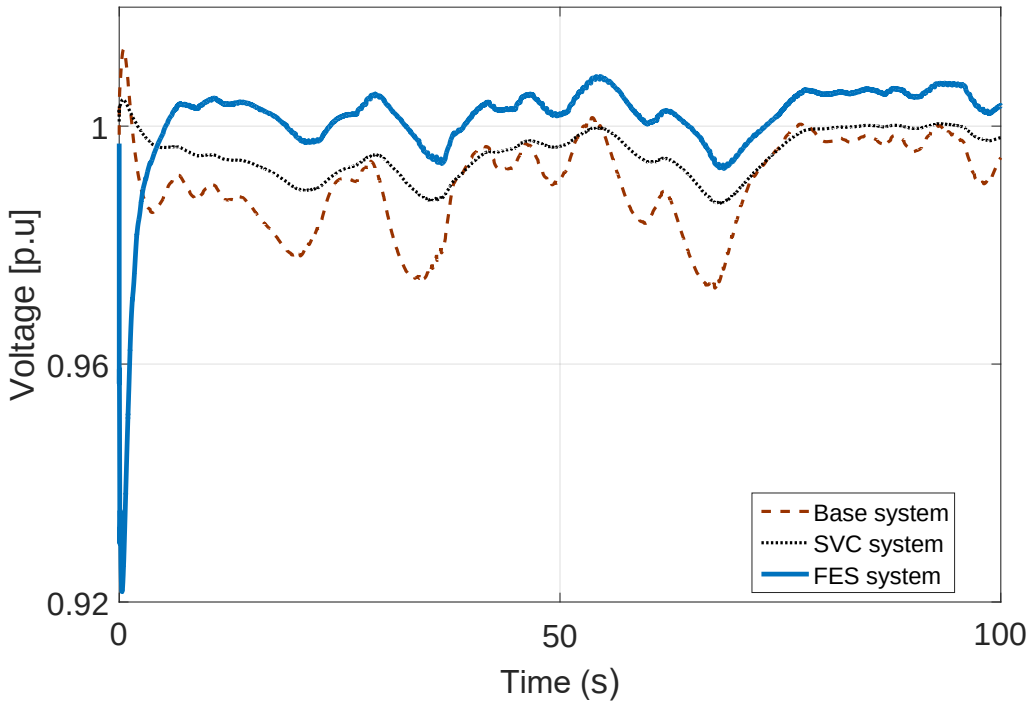

Figure 4.12: Voltage profile at Bus 1.

4.2.3 Synchronous Generator Mechanical Torque

The mechanical torque of the synchronous generator varies considerably in the Base system, while its variation is reduced in the FES system, due to the contribution of the FES active power to frequency control, as seen in Figure 4.13.

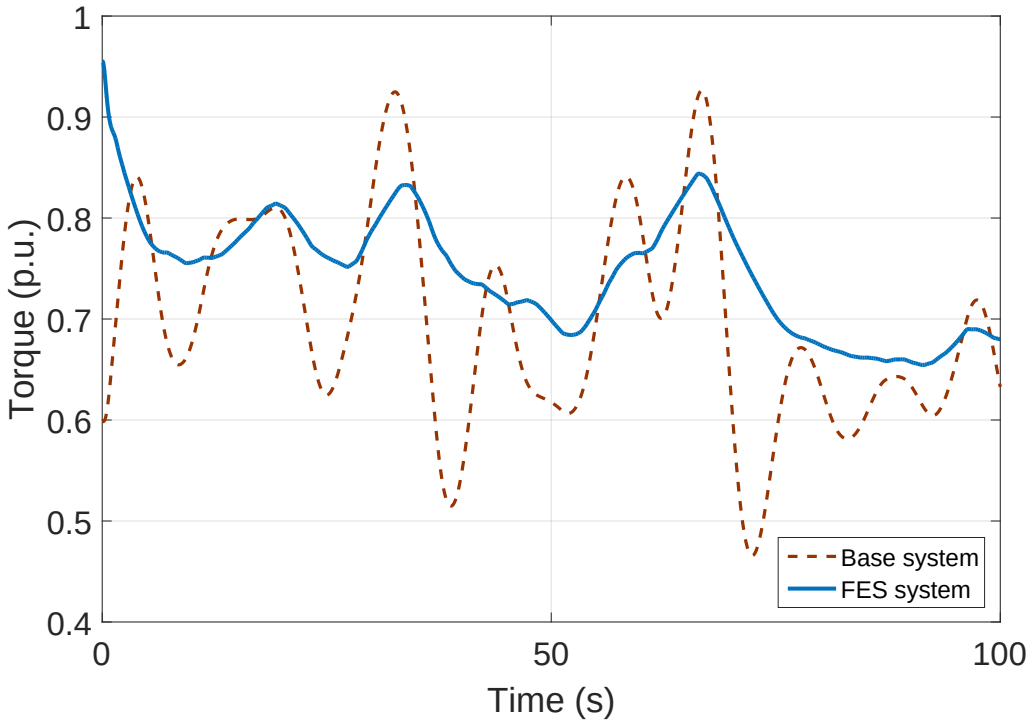

Figure 4.13: Synchronous generator mechanical torque.

4.2.4 FES Active Power and Speed

From Figure 4.14 it can be noticed that the proposed FES has a very fast response and ramp rate, with matches its high energy density characteristics, which is essential for high power, low energy applications. Observe also in Figure 4.15, that the proposed FES is capable to transition from discharge to charge mode (generator to motor mode) within only a few seconds.

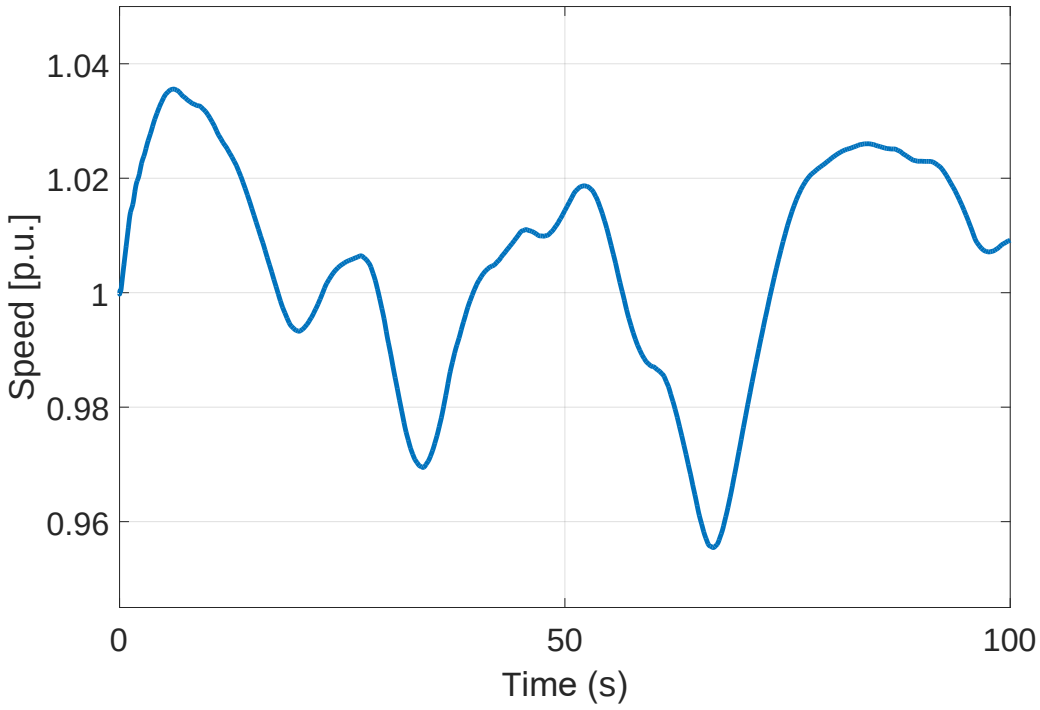

Figure 4.14: FES rotational speed.

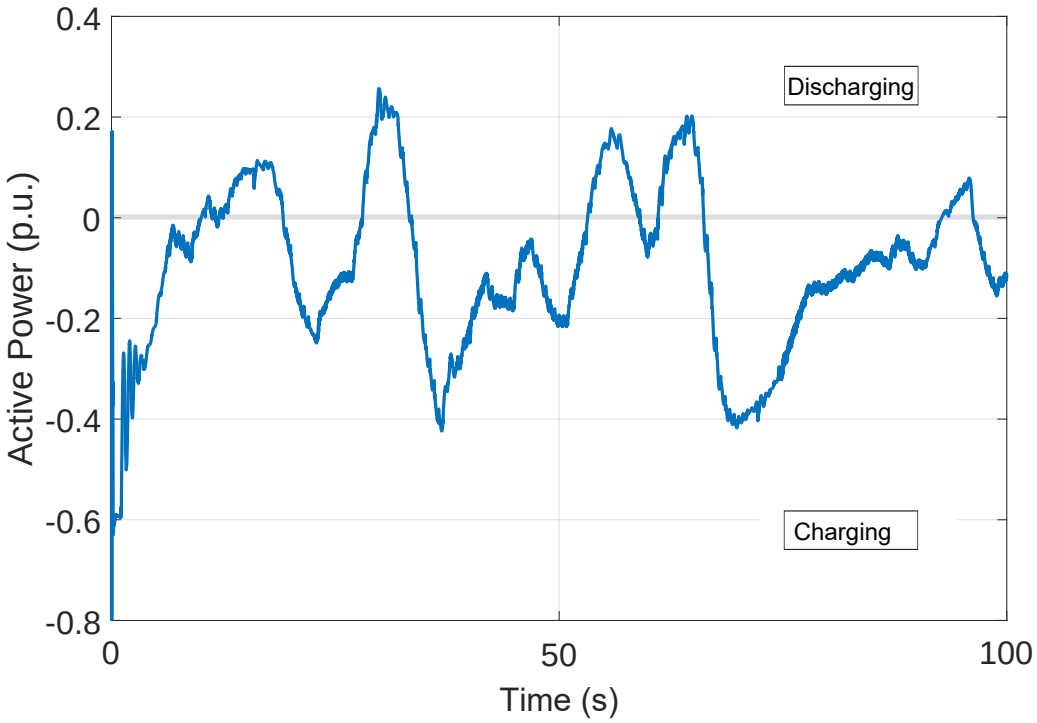

Figure 4.15: FES active power.

4.2.5 Results Comparison and Validation

The system frequency response, voltage profile, and synchronous mechanical torque plots, and also the WES and FES behavior, presented in this work for the Base and FES systems are compared here to the results presented in [28] for the first 100s, where 3-phase detailed PSCAD/EMTDC models where used. In Figures 4.16-4.21, the results obtained from the simulations in DSATools® are shown on the left side of each figure (i.e. part a), whereas the results extracted from [28] are on the right side (i.e. part b); the plots are presented using the same scale for comparison purposes. Notice the similarities of the results, which basically validate the proposed DSATools® models.

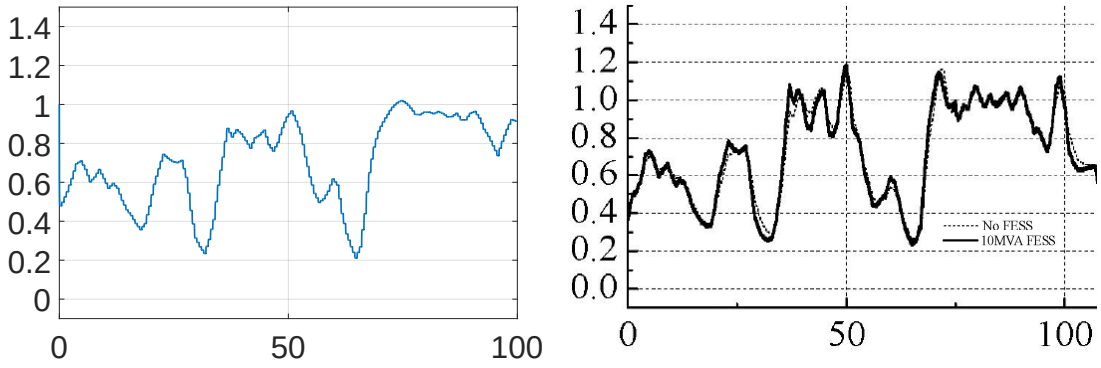

(a) (b) [28]

Figure 4.16: Wind active power.

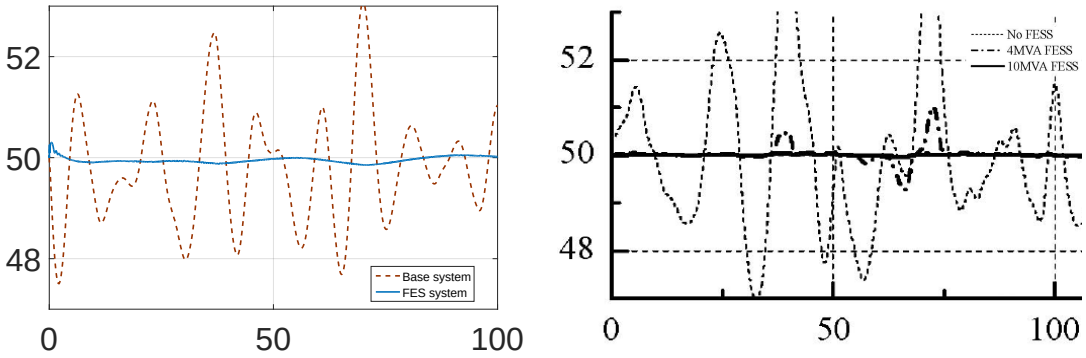

(a) (b) [28]

Figure 4.17: System frequency.

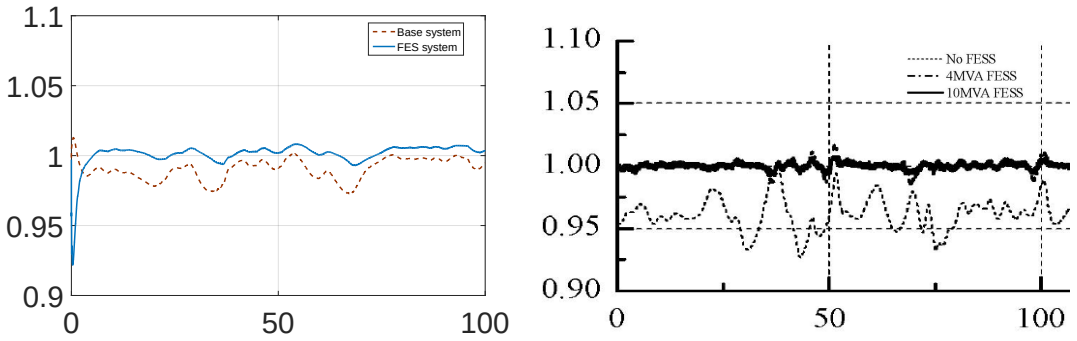

(a) (b) [28]

Figure 4.18: Voltage profile

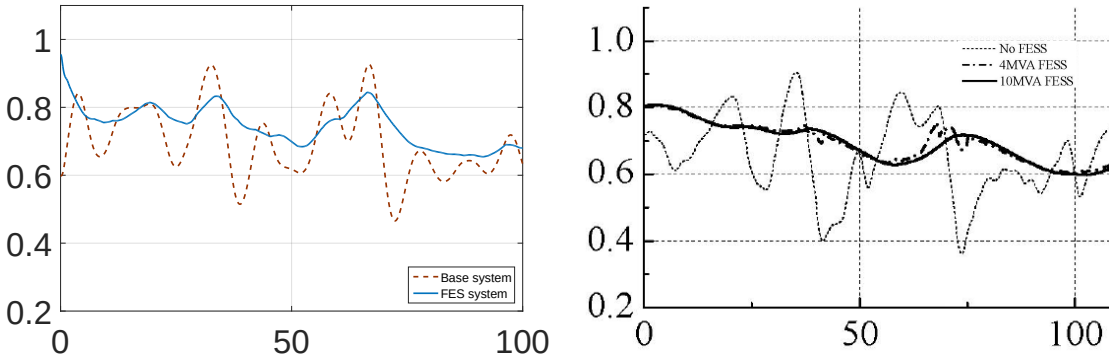

(a) (b) [28]

Figure 4.19: Synchronous generator mechanical torque.

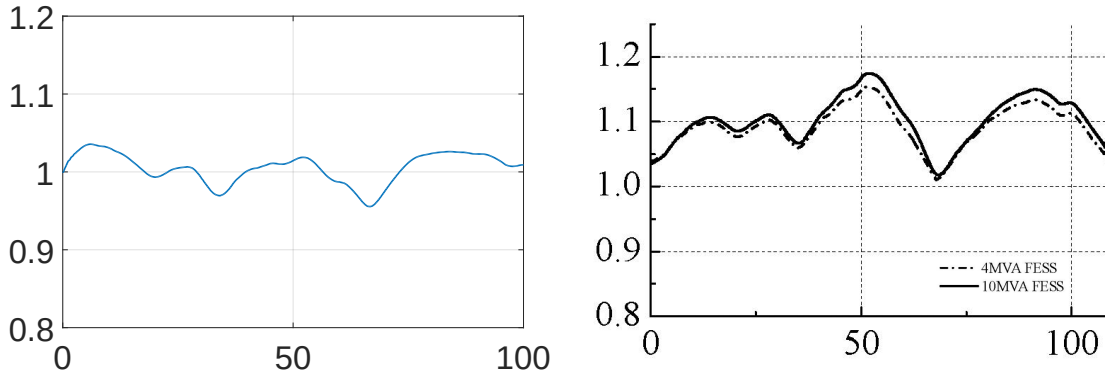

(a) (b) [28]

Figure 4.20: FES speed.

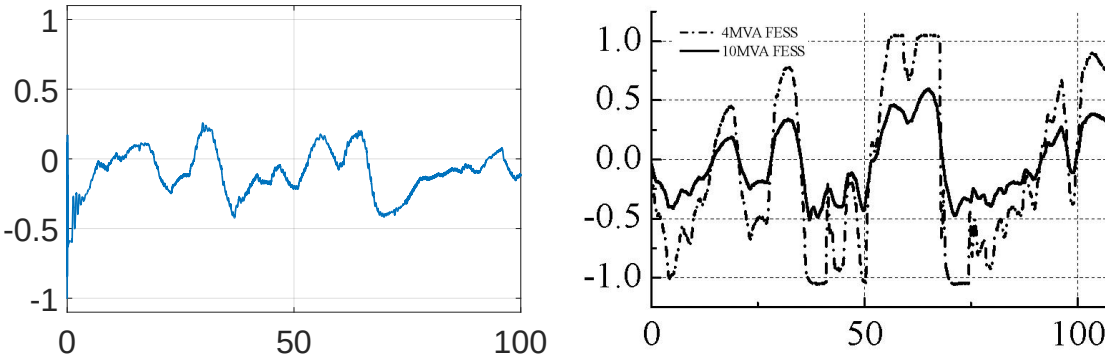

(a) (b) [28]

Figure 4.21: FES active power.

4.3 Summary

This chapter presented the application of the FES system model discussed in Chapter 3 to provide PFC. Three system configurations, the Base system, an SVC system, and an FES system were considered for the studies. Detailed descriptions of the models and parameters for each of the components used in the three study cases were provided. The results were

compared with the plots presented in [28] and their affiniti with the results presented in this thesis validated the DSATools® models, and demostrated that the FES system provided an efficient PFC service, with a significant improvement in frequency response due to the FES for PFC, and an optimal compensation of the WES active power fluctuaction; also, the FES system was able to provide an adequate voltage regulation compared with the SVC control.

Chapter 5

Conclusions, Contributions and Future Work

5.1 Summary and Conclusions

The research presented in this thesis focused on PFC in a power system using a practical FES system model, to damp the frequency fluctuations arising from wind speed variation in high-capacity WES. Three different study cases were carried out on an existing test system, used here as a benchmark for validation purposes, demonstrating the effectiveness of the proposed FES model.

In chapter 2, the mathematical background required for the development of frequency controls was presented, followed by an overview of ESS for power system applications focusing on BESS. A synopsis of FES systems was given, outlining their main characteristics and configuration, and discussing their suitability for PFC. Finally, the main features of the software DSATools® and its core programs, used here to develop a practical FES model, were presented.

In Chapter 3, the structure and details of the proposed FES model were provided. Thus, a detailed description of all the components included in the FES system, along with their DSATools® models, were presented. Furthermore, the controls implemented for each component, and their parameters, were described.

In Chapter 4, the configurations of the three case studies were presented, together with their components, controls, and parameters. Thereafter, dynamic performance analyses in response of fast fluctuations in wind speed, focusing on frequency response, voltage profiles,

power outputs, and other relevant variables for all cases, were provided, followed by an evaluation of the FES performance with respect to rotor speed and charging/discharging operation.

The main conclusions and findings of this thesis are the following:

- The proposed FES system model for PFC properly represented the steady state and dynamic response expected of FES, in particular with respect to its fast-response, high active power ramp rates, and flexibility of operation characteristics.
- The results obtained from the implementation of the proposed FES system model demonstrated the adequacy of these systems for PFC and voltage regulation.
- It was shown that FES can reduce the variation of a synchronous generator mechanical torque, since the active power fluctuations of the WES system can be compensated by the FES, instead of the synchronous generator.

5.2 Contributions

The contributions of the presented research are the following:

- Developed and validated a dynamic model of a FES for the popular DSATools®, used by the IESO, to assess its impact on PFC performance.
- Implemented a state-of-art frequency and voltage control strategy in a converter based FES model, considering the FES speed limiter, frequency deviation, and converter voltage controller.
- Demonstrated and studied frequency and voltage variations and control, and FES characteristics and performance in the realistic test system extracted from [28], with significant wind power penetration and variations.

5.3 Future Work

Based on the work presented in this thesis, future research may explore the following subjects:

- The presented FES system model could be further validated based on the performance of an existing FES installation, which could be used to improve the model.
- Further studies with the proposed FES system model could be carried out to analyze other possible services such as the response to fast regulation signals from power system operators.
- Study the impact of the presented FES system model in Ontario's power grid in the provision of ancillary services.

References

[1] P. Kundur, N. J. Balu, and M. G. Lauby, *Power system stability and control*. McGraw-Hill New York, 1994, vol. 7.

[2] "IESO supply overview," http://www.ieso.ca/Pages/Power-Data/Supply.aspx, IESO, June 2017.

[3] J. A. Taylor, D. S. Callaway, and K. Poolla, "Competitive energy storage in the presence of renewables," *IEEE Transactions on Power Systems*, vol. 28, no. 2, pp. 985–996, 2013.

[4] "NRStor Minto flywheel energy storage project," http://www.energystorageexchange.org/projects/769, U.S. Department of Energy.

[5] "RES Amphora battery energy storage project," http://www.energystorageexchange.org/projects/1448, U.S. Department of Energy.

[6] "IESO report: Energy storage," IESO, Tech. Rep., March 2016. [Online]. Available: http://www.ieso.ca/en/sector-participants/ieso-news/2016/03/technical-report-on-energy-storage-available-on-ieso-website

[7] M. A. Awadallah and B. Venkatesh, "Energy storage in flywheels: An overview," *Canadian Journal of Electrical and Computer Engineering*, vol. 38, no. 2, pp. 183–193, Spring 2015.

[8] K. Vidyanandan and N. Senroy, "Frequency regulation in a wind–diesel powered microgrid using flywheels and fuel cells," *IET Generation, Transmission & Distribution*, vol. 10, no. 3, pp. 780–788, 2016.

[9] G. Delille, B. François, and G. Malarange, "Dynamic frequency control support by energy storage to reduce the impact of wind and solar generation on isolated power

system's inertia," *IEEE Transactions on Sustainable Energy*, vol. 3, no. 4, pp. 931–939, Oct 2012.

[10] L. Wu, W. Gao, Z. Cui, and X. Kou, "A novel frequency regulation strategy with the application of energy storage system for large scale wind power integration," in *Proc. Seventh Annual IEEE Green Technologies Conference*, April 2015, pp. 221–226.

[11] H. Ye, Z. Qi, and W. Pei, "Modeling and evaluation of short-term frequency control for participation of wind farms and energy storage in power systems," in *Proc. International Conference on Power System Technology*, Oct 2014, pp. 2647–2654.

[12] P. Mercier, R. Cherkaoui, and A. Oudalov, "Optimizing a battery energy storage system for frequency control application in an isolated power system," *IEEE Transactions on Power Systems*, vol. 24, no. 3, pp. 1469–1477, Aug 2009.

[13] M. Khalid and A. Savkin, "An optimal operation of wind energy storage system for frequency control based on model predictive control," *Renewable Energy*, vol. 48, pp. 127–132, 2012.

[14] D. I. Stroe, V. Knap, M. Swierczynski, A. I. Stroe, and R. Teodorescu, "Operation of a grid-connected lithium-ion battery energy storage system for primary frequency regulation: A battery lifetime perspective," *IEEE Transactions on Industry Applications*, vol. 53, no. 1, pp. 430–438, Jan 2017.

[15] P. Prajapati and A. Parmar, "Multi-area load frequency control by various conventional controller using battery energy storage system," in *Proc. International Conference on Energy Efficient Technologies for Sustainability (ICEETS)*, April 2016, pp. 467–472.

[16] M. Koller, T. Borsche, A. Ulbig, and G. Andersson, "Review of grid applications with the Zurich 1MW battery energy storage system," *Electric Power Systems Research*, vol. 120, pp. 128–135, 2015.

[17] M. Świerczyński, D. I. Stroe, A. I. Stan, and R. Teodorescu, "Primary frequency regulation with li-ion battery energy storage system: A case study for Denmark," in *Proc. IEEE ECCE Asia Downunder*, June 2013, pp. 487–492.

[18] N. T. Janssen, R. A. Peterson, and R. W. Wies, "Improved frequency regulation on hybrid wind-diesel microgrids using self-sensing electric thermal storage devices," in *Proc. Australasian Universities Power Engineering Conference (AUPEC)*, Sept 2014, pp. 1–6.

[19] A. A. K. Arani and G. B. Gharehpetian, "Enhancement of microgrid frequency control subsequent to islanding process using flywheel energy storage system," in *Proc. Smart Grid Conference (SGC)*, Dec 2014, pp. 1–6.

[20] M. L. Lazarewicz and T. M. Ryan, "Integration of flywheel-based energy storage for frequency regulation in deregulated markets," in *Proc. IEEE PES General Meeting*, July 2010, pp. 1–6.

[21] A. R. Ahmadi, F. Ghardashi, D. Kabiri, A. Sheykholeslami, and H. Haeri, "Voltage and frequency control in smart distribution systems in presence of DER using flywheel energy storage system," in *Proc. 22nd International Conference and Exhibition on Electricity Distribution (CIRED 2013)*, June 2013, pp. 1–4.

[22] F. Zhang, M. Tokombayev, Y. Song, and G. Gross, "Effective flywheel energy storage (FES) offer strategies for frequency regulation service provision," in *Proc. Power Systems Computation Conference*, Aug 2014, pp. 1–7.

[23] X.-D. Sun, K.-H. Koh, B.-G. Yu, and M. Matsui, "Fuzzy-logic-based v/f control of an induction motor for a dc grid power-leveling system using flywheel energy storage equipment," *IEEE Transactions on Industrial Electronics*, vol. 56, no. 8, pp. 3161–3168, 2009.

[24] X. Li, S. Tan, J. Huang, Y. Huang, M. Wang, T. Xu, and X. Cheng, "Optimal sizing for flywheel energy storage system-conventional generator coordination in load frequency control," in *Proc. International Conference on Power System Technology*, Oct 2014, pp. 582–587.

[25] R. G. Said, A. S. Abdel-Khalik, A. E. Zawawi, and M. S. Hamad, "Integrating flywheel energy storage system to wind farms-fed hvdc system via a solid state transformer," in *Proc. International Conference on Renewable Energy Research and Application (ICRERA)*, Oct 2014, pp. 375–380.

[26] G. Cimuca, S. Breban, M. M. Radulescu, C. Saudemont, and B. Robyns, "Design and control strategies of an induction-machine-based flywheel energy storage system associated to a variable-speed wind generator," *IEEE Transactions on Energy Conversion*, vol. 25, no. 2, pp. 526–534, June 2010.

[27] H. Silva-Saravia, H. Pulgar-Painemal, and J. M. Mauricio, "Flywheel energy storage model, control and location for improving stability: The Chilean case," *IEEE Transactions on Power Systems*, vol. 32, no. 4, pp. 3111–3119, July 2017.

[28] R. Takahashi and J. Tamura, "Frequency stabilization of small power system with wind farm by using flywheel energy storage system," in *Proc. IEEE International Symposium on Diagnostics for Electric Machines, Power Electronics and Drives*, Sept 2007, pp. 393–398.

[29] P. Kundur, J. Paserba, V. Ajjarapu, G. Andersson, A. Bose, C. Cañizares, N. Hatziargyriou, D. Hill, A. Stankovic, C. Taylor, T. V. Cutsem, and V. Vittal, "Definition and classification of power system stability IEEE/CIGRE joint task force on stability terms and definitions," *IEEE Transactions on Power Systems*, vol. 19, no. 3, pp. 1387–1401, Aug 2004.

[30] "Balancing and frequency control," http://www.nerc.com/docs/oc/rs/NERC%20Balancing%20and%20Frequency%20Control%20040520111.pdf, NERC.

[31] N. Miller, M. Shao, S. Pajic, and R. D'Aquila, "Eastern frequency response study," National Renewable Energy Laboratory (NREL), Golden, CO., Tech. Rep., 2013.

[32] L. Xie, A. A. Thatte, and Y. Gu, "Multi-time-scale modeling and analysis of energy storage in power system operations," in *Proc. IEEE 2011 EnergyTech*, May 2011, pp. 1–6.

[33] W. Du, H. Wang, L. Xiao, and R. Dunn, "Modeling energy storage systems into electric power transmission systems," in *Proc. 44th International Universities Power Engineering Conference (UPEC)*, Sept 2009, pp. 1–5.

[34] P. F. Ribeiro, B. K. Johnson, M. L. Crow, A. Arsoy, and Y. Liu, "Energy storage systems for advanced power applications," *Proceedings of the IEEE*, vol. 89, no. 12, pp. 1744–1756, Dec 2001.

[35] R. Carnegie, D. Gotham, D. Nderitu, and P. V. Preckel, "Utility scale energy storage systems," *State Utility Forecasting Group. Purdue University*, vol. 1, 2013.

[36] I. Dincer and M. Rosen, *Thermal energy storage: systems and applications*. John Wiley & Sons, 2002.

[37] K. Divya and J. Østergaard, "Battery energy storage technology for power systems an overview," *Electric Power Systems Research*, vol. 79, no. 4, pp. 511–520, 2009.

[38] A. Green, "The characteristics of the nickel-cadmium battery for energy storage," *Power Engineering Journal*, vol. 13, no. 3, pp. 117–121, June 1999.

[39] E. Thorbergsson, V. Knap, M. Swierczynski, D. Stroe, and R. Teodorescu, "Primary frequency regulation with li-ion battery based energy storage system - evaluation and comparison of different control strategies," in *Proc. 35th International Telecommunications Energy Conference*, Oct 2013, pp. 1–6.

[40] N. Mohan, T. M. Undeland, and W. P. Robbins, *Power electronics: converters, applications, and design*. John Wiley & Sons, 2003.

[41] J. i. Itoh, D. Sato, T. Nagano, K. Tanaka, N. Yamada, and K. Kato, "Development of high efficiency flywheel energ storage system for power load-leveling," in *Proc. IEEE 36th International Telecommunications Energy Conference (INTELEC)*, Sept 2014, pp. 1–8.

[42] VYCON, "Energy storage, flywheel battery-free UPS, active magnetic bearing, magnetic bearings, kinetic energy, magnet motor generator, bi-directional power converter — calnetix," http://www.calnetix.com/vdc-kinetic-energy-storage-systems.

[43] T. D. Nguyen, K. J. Tseng, S. Zhang, and H. T. Nguyen, "On the modeling and control of a novel flywheel energy storage system," in *Proc. IEEE International Symposium on Industrial Electronics*, July 2010, pp. 1395–1401.

[44] G. Genta, *Kinetic energy storage: theory and practice of advanced flywheel systems*. Butterworth-Heinemann, 2014.

[45] F. Biggs, "Flywheel energy systems," *NASA STI/Recon Technical Report N*, vol. 75, 1974.

[46] S. Simard, K. Fytas, J. Paraszczak, M. Laflamme, and K. Agbossou, "Wind power opportunities for remote mine sites in the Canadian North," *Renewable Energy and Power Quality Journal*, vol. 01, no. 15, April 2017.

[47] *PSAT Manual*, 16th ed., Powertech Labs Inc., April 2016.

[48] *TSAT Manual*, 16th ed., Powertech Labs Inc., April 2016.

[49] *DSA UDM Manual*, 16th ed., Powertech Labs Inc., April 2016.